UNIVERSITAT POLITÈCNICA DE CATALUNYA

ENGINYERIA EN TECNOLOGIES AEROESPACIALS (GRETA)

Jordi LLAURADÓ COSTA

Study of buckling phenomena for *SMART* structural applications

Director:
Joaquín Alberto HERNÁNDEZ ORTEGA

30th June, 2020

UNIVERSITAT POLITÈCNICA DE CATALUNYA
BARCELONATECH
Escola Tècnica Superior d'Enginyeries
Industrial i Aeronàutica de Terrassa

Contents

1 Introduction

1.1 Abstract

This project analyses the structural instability known as buckling, both from a displacement and energy point of view. In order to do so, first of all, a time integration method is implemented and checked to be properly functioning. Next, a mass-spring-damper model is modified to accurately represent the behaviour of a buckling system. This system is later on studied both using a displacement-controlled and a force-controlled analysis, as each one offers different outcomes. Besides, once these studies have been carried out, an analysis of a chain of multiple springs will be performed, as it could represent the behaviour of a more complex structure such as shape memory alloys. The results obtained in this project coincide with the ones expected, both in terms of energy dissipation and displacement. In the force-controlled analysis the snap-through phenomena is shown, meanwhile the snap-back phenomena takes place in the displacement-controlled analysis. Besides, the chain of multiple springs does indeed represent the pseudoelasticity shown in the stress-strain diagram of *SMART* materials such as Nitinol. To sum up, it has been found that rather than being only avoided as it is an indicative of instability, the buckling phenomena and the post-buckling behaviour might actually have some useful applications.

Este proyecto analiza la inestabilidad estructural conocida como pandeo, centrándose en ambos el estudio energético y la evolución del desplazamiento. Para llevar a cabo dicho análisis, en primer lugar un método de integración temporal es implementado, y se corrobora su correcto funcionamiento. A continuación, un modelo masa-resorte-amortiguador es modificado para representar de forma precisa el comportamiento de un sistema bajo pandeo. Este sistema es estudiado utilizando ambos, un análisis bajo fuerza controlada y otro bajo desplazamiento controlado, ya que cada uno debería ofrecer resultados diferentes. Además, una vez dichos estudios se hayan realizado, una cadena de múltiples muelles consecutivos es analizada, ya que podría representar el comportamiento de estructuras más complejas como las aleaciones con memoria de forma. Los resultados obtenidos en este proyecto coinciden con los esperados, tanto en términos energéticos como en el desplazamiento. En el análisis con fuerza controlada se muestra el fenómeno conocido como *snap-through*, mientras que el fenómeno llamado *snap-back* se manifiesta en el análisis con desplazamiento controlado. Asimismo, la cadena hecha de varios muelles representa la superplasticidad mostrada en el diagrama de tensión-deformación de un material inteligente como por ejemplo el Nitinol. En conclusión, ha sido demostrado que, en lugar de ser evitado ya que es un indicativo de inestabilidad, el fenómeno del pandeo y el comportamiento que lo sigue puede tener aplicaciones útiles.

1.2 Aim of the project

- Understanding of a meta-stable/bi-stable material behaviour (both in energy and displacement fields).
- Plausible applications of meta-stable/bi-stable elements.

1.3 Scope

- Modal analysis of a both a free vibration (undamped and damped) as well as a forced vibration (damped).
- Implementation of two time integration methods (Runge Kutta and Newmark) and its validation using the modal solution developed previously.
- Reliability of the time integration methods using a non-linear spring (exponential spring).
- Forced-controlled analysis of a mass-spring-damper model simulating a meta-stable/bi-stable element (displacement and energy results).
- Displacement-controlled analysis of a mass-spring-damper model simulating a meta-stable/bi-stable element (displacement and energy results).
- Analysis of a meta-stable/bi-stable element chain.

1.4 Requirements

- Snap-through and snap-back phenomena representation using the simulated mass-spring-damper model.
- Energy dissipated during an hysteresis cycle (loading-unloading).
- Behaviour of a chain made of bi-stable/meta-stable elements.

1.5 Justification and utility

Buckling has always been avoided as it is an indicative of a collapsing structure. However, this new standpoint in which a structure made of buckling elements can present more than one stable state is really promising. [1]

Despite being on early stages of its development, buckling induced structures have already been implemented in both relatively simple structures [2] [3] and more complex ones [4], such as morphing wings. [5] [6]

Focusing on the later, an aircraft wing is put under multiple loading situations during a flight. In order to make the structure the most effective possible, moving parts have been implemented such as flaps. Nonetheless, these moving structures require high-level engineering and they have a costly maintenance. A wing capable of changing its shape mid-flight depending on the load conditions would be a major leap in the aircraft industry. Furthermore, it would suppose the end of these expensive mobile structures.

Moreover, it has been studied [7] that a bi-stable/meta-stable chain could potentially represent the behaviour of *SMART* materials such as Nitinol [8], both in terms of super elasticity and shape memory. Therefore, in this project it will be attempted to recreate this behaviour.

2 Development

2.1 State of the art

To begin with, in the latest years there has been a change on the perspective of structural instabilities (such as buckling, wrinkling and phase transformation). In this case the focus will be placed on the buckling instability. Buckling has always been avoided during the development of a structure, but recently this behaviour has been determined as favorable in certain scenarios. What once was not given much attention, now is being thoroughly studied.

This newly arisen trend is focused on studying nonlinear materials, also called *SMART* materials or meta-materials [9]. These materials present meta-stable or bi-stable structural elements, which means that they have multiple stable positions or two stable positions, respectively. To illustrate the bi-stable behaviour, a simple buckling example is explained below.

Imagine a clamped beam of longitude d in a gap of width L, being d greater than L ($d > L$). In this situation the beam would show a buckling behaviour as depicted in Figure 1

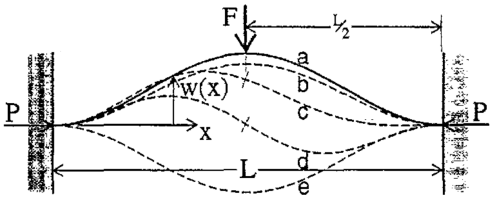

Figure 1: Depiction of a buckled beam. Extracted from [10]

If a constantly increasing force F is applied on the middle of the beam, the beam would eventually snap to the down position in a sudden way. If the force is then gradually removed, the beam doesn't return to its original placement (the first stable position) and remains in the down position (the second stable position). These two stable positions are shown in the image below.

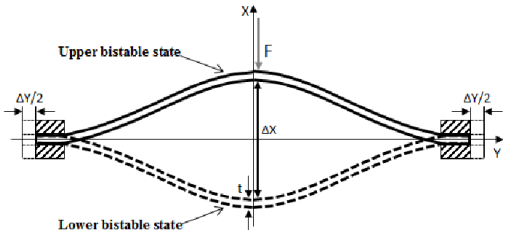

Figure 2: Representation of the two stable states that a buckled beam presents, the upper and the lower ones. Extracted from [10]

This behaviour brings up multiple fields in which the use of bi-stable (and meta-stable) materials would be very beneficial. Until now, post-buckling response has never been considered important as it was thought to not offer any practical applications (as it highly depends on the initial conditions). However, in the

elastic region, structures are capable of quickly snapping from its initial position to a buckled state. Both the sudden change in position and the energy released during this change are useful features for *SMART* applications. Therefore, the use of the buckling phenomena is mainly split between two: energy-related applications and motion-related applications.

The former can be once again split into two: energy generation and energy dissipation. On the one hand, the energy released during a buckling phenomena can be then used to design sensors for micro-electromechanical systems and energy harvesters. On the other hand, the dissipated energy phenomena that takes place during a buckling event might be useful to design dampers, absorbers and isolators.

The latter is based on the quick change in position that happens in snap-through. A small perturbation in a structure made up of multiple buckling elements can produce a drastic change on the overall structure geometry.

The internal force evolution during the snap produced in the clamped beam explained above is depicted below, in Figure 3.

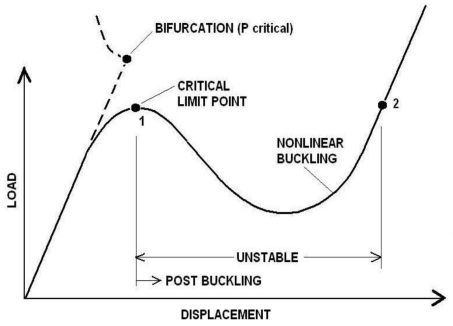

Figure 3: Equilibrium paths for nonlinear and bifurcation buckling. Extracted from [11]

As it can be seen, the internal force behaves similar to a polynomial function of grade 3. It reaches up to a maximum point (critical point) and then decreases to a minimum value, followed again by another increase.

The difference between a meta-stable mechanism and a bi-stable mechanism is that, in the former, the lowest value of the internal force is positive, meanwhile in the latter the lowest value of the internal force is positive. [12] [2] This difference is shown in Figure 4.

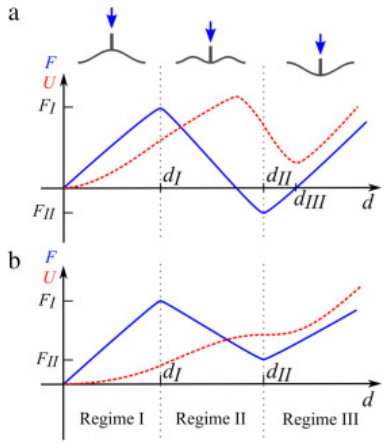

Figure 4: (a) Schematic representations for the force–displacement (F–d) behavior and change of potential energy (U) as function of displacement for a bi-stable mechanism, and for (b) a meta-stable mechanism. Extracted from [2]

An assembly of bi-stable elements offer morphing structures, which have two stable states. An example of these morphing structures can be seen in Figure 5.

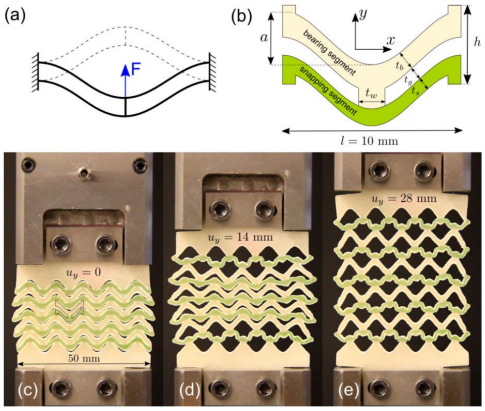

Figure 5: Figures a) and b) show the bi-stable element the system is made up of. Figures c) and e) show the two stable positions, being d) the transitory state. Extracted from [13]

2.2 Proposed approach and alternative choice

First of all, all this project will be developed around a mass-spring-damper model. This model can be seen in Figure 6.

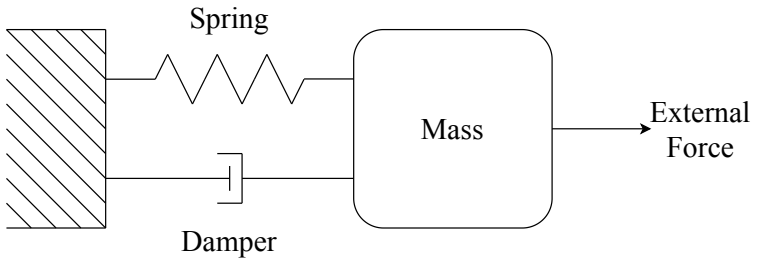

Figure 6: Simple mass-spring-damper system

From here, firstly a modal analysis of the most simple cases will be performed. Once this is done, two time-integration methods using *MATLAB* software will be developed (Runge-Kutta and Newmark), and their results will be compared with the ones obtained from the modal solution, in order to check the reliability of this integration methods.

Secondly, a system with a non-linear spring (exponential) will be analyzed using both time integration methods, in order to prove that they work in non-linear scenarios.

Thirdly, a piecewise spring will be developed in order to resemble the one shown in Figure 3. This spring is shown in the following section.

2.2.1 Piecewise linear spring

The developed piecewise linear spring will have the following behaviour: the internal force will grow up to a point (F_{max}) at which it will start decreasing until it reaches a lower value (F_{min}) and from there it will increase again but at a different pace (k_1) than the first section (k_0) [14]. This piecewise behaviour is shown in Equation 1

$$F_{int}(x) = \begin{cases} k_0 \cdot x & 0 \leq x < x_{max} \\ F_{max} - k_0 \cdot (x - x_{max}) & x_{max} \leq x < x_{min} \\ F_{min} + k_1 \cdot (x - x_{min}) & x_{min} \leq x \end{cases} \tag{1}$$

Whether the system will be classified as meta-stable or bi-stable depends on the lower value of the force (F_{min}) [2], the first one will have a positive value, meanwhile the second one will have a negative one.

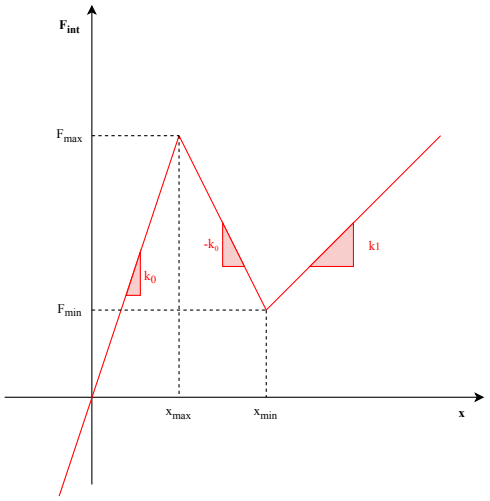

Figure 7: Piecewise spring behaviour

After this, a study of a system implementing the piecewise linear behaviour will be performed, both in force-controlled and displacement-controlled scenarios. Both studies are being done as in the former the snap-through phenomena will be shown, while in the later the snap-back will be displayed. [15]

Finally, to conclude, a chain of multiple springs will be analyzed (displacement-controlled analysis).

3 Development of the proposed solution

First of all, a simple mass-spring-damper model will be studied using *MATLAB* software to work out its response in time. Three different conditions will be considered, as shown in figure 8. Each one of these cases will be analyzed using a modal analysis, followed by a time integration.

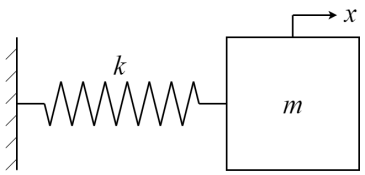

(a) Free undamped vibration

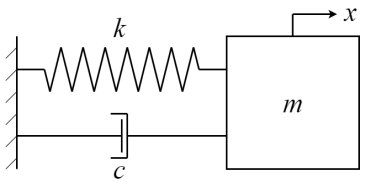

(b) Free damped vibration

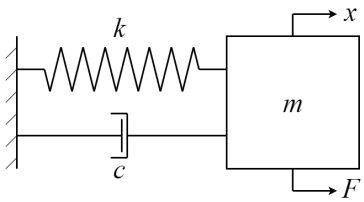

(c) Forced (harmonic force) damped vibration

Figure 8: Mechanical schemes of the three different conditions under which the system will be analyzed

3.1 Modal Analysis

First of all, a modal analysis will be performed in order to verify the accuracy of the time integration methods used along this project.

3.1.1 Case 1: Free undamped vibration

The equation of motion that describes the conditions in Figure 8a is as follows

$$m\ddot{x} = -kx \tag{2}$$

Using an harmonic solution with the form

$$x(t) = Xe^{\omega it} = Xe^{st} \tag{3a}$$

$$\dot{x}(t) = X\omega ie^{\omega it} = Xse^{st} \tag{3b}$$

$$\ddot{x}(t) = -X\omega^2 e^{\omega it} = Xs^2 e^{st} \tag{3c}$$

By replacing Equation 3a and Equation 3c in the equation of motion Equation 2, and reorganizing the equation terms, the following is obtained.

$$Xe^{st}(k + ms^2) = 0 \tag{4}$$

By isolating s from Equation 4, the two values are obtained.

$$s_{1,2} = \pm\sqrt{-\frac{k}{m}} = \pm i\sqrt{\frac{k}{m}} \tag{5}$$

As $s = \omega i$, then $\omega = \pm\sqrt{\frac{k}{m}}$, being these the natural frequencies of the system (ω_n). The solution of Equation 2 is the sum of the contributions of each mode (the positive and negative one).

$$x = X_1 e^{\omega_n i t} + X_2 e^{-\omega_n i t} \tag{6a}$$

$$\dot{x} = \omega_n i (X_1 e^{\omega_n i t} - X_2 e^{-\omega_n i t}) \tag{6b}$$

To determine the values of X_1 and X_2 the initial conditions are applied ($t = 0$), both for the position and the velocity. Therefore the following system of equations is obtained.

$$\begin{aligned} x_0 &= X_1 + X_2 \\ \dot{x}_0 &= \omega_n i (X_1 - X_2) \end{aligned} \tag{7}$$

The solutions of which are

$$\boxed{X_1 = \frac{x_0\omega_n - \dot{x}_0 i}{2\omega_n} \qquad X_2 = \frac{x_0\omega_n + \dot{x}_0 i}{2\omega_n}}$$

Alternately, the values of X_1 and X_2 can be expressed in the exponential form ($X = Ae^{i\beta}$). To do so, first of all the imaginary and real parts of each one have to be identified.

$$\mathrm{Re}(X_1) = \frac{x_0}{2} \qquad \mathrm{Im}(X_1) = \frac{-\dot{x}_0}{2\omega_n} \tag{8a}$$

$$\mathrm{Re}(X_2) = \frac{x_0}{2} \qquad \mathrm{Im}(X_2) = \frac{\dot{x}_0}{2\omega_n} \tag{8b}$$

Then, the values of A and β are worked out as follows:

$$A_1 = \sqrt{\mathrm{Re}(X_1)^2 + \mathrm{Im}(X_1)^2} = \sqrt{\frac{(x_0\omega_n)^2 + \dot{x}_0^2}{4\omega_n^2}} = A \quad \beta_1 = \arctan\frac{\mathrm{Im}(X_1)}{\mathrm{Re}(X_1)} = \arctan\frac{-\dot{x}_0}{x_0\omega_n} = \beta \tag{9a}$$

$$A_2 = \sqrt{\mathrm{Re}(X_2)^2 + \mathrm{Im}(X_2)^2} = \sqrt{\frac{(x_0\omega_n)^2 + \dot{x}_0^2}{4\omega_n^2}} = A \quad \beta_2 = \arctan\frac{\mathrm{Im}(X_2)}{\mathrm{Re}(X_2)} = \arctan\frac{\dot{x}_0}{x_0\omega_n} = -\beta \tag{9b}$$

Therefore, taking into account the trigonometry identities ($\sin[-a] = -\sin a$, $\cos[-a] = \cos a$) and Euler's identity ($e^{\theta i} = \cos\theta + i\sin\theta$), Equation 3a can be rewritten as

$$x = Ae^{i\beta}e^{i\omega_n t} + Ae^{-i\beta}e^{-i\omega_n t} = 2A\cos(\omega_n + \beta) \tag{10}$$

To finish with, the solution to the free undamped system is

$$\boxed{x(t) = 2A\cos(\omega_n + \beta)} \tag{11}$$

Where

$$A = \sqrt{\frac{(x_0\omega_n)^2 + \dot{x}_0^2}{4\omega_n^2}}$$
$$\beta = \arctan\frac{-\dot{x}_0}{x_0\omega_n}$$

3.1.2 Case 2: Free damped vibration

The equation of motion that describes the conditions in Figure 8b is as follows.

$$m\ddot{x} = -kx - c\dot{x} \tag{12}$$

Using an harmonic solution with the shape

$$x(t) = Xe^{\omega it} = Xe^{st} \tag{13a}$$
$$\dot{x}(t) = X\omega ie^{\omega it} = Xse^{st} \tag{13b}$$
$$\ddot{x}(t) = -X\omega^2 e^{\omega it} = Xs^2 e^{st} \tag{13c}$$

By replacing Equation 13a, Equation 13b and Equation 13c in the equation of motion Equation 12, and reorganizing the equation terms, the following is obtained.

$$Xe^{st}(k + cs + ms^2) = 0 \tag{14}$$

The solution of which, yields the following values of s

$$s_{1,2} = -\frac{c}{2m} \pm \sqrt{\left(\frac{c}{2m}\right)^2 - \frac{k}{m}} \tag{15}$$

By reorganizing Equation 15, the following equation is obtained.

$$s_{1,2} = -\frac{c}{2\sqrt{km}}\sqrt{\frac{k}{m}} \pm \sqrt{\frac{k}{m}}\sqrt{\frac{c^2}{4mk} - 1} = -\zeta\omega_n \pm \omega_n\sqrt{\zeta^2 - 1} \tag{16}$$

Where

$$\omega_n \text{ is the natural frequency.} \quad \omega_n = \sqrt{\frac{k}{m}}$$
$$\zeta \text{ is the damping ratio} \quad \zeta = \frac{c}{2\sqrt{km}}$$

Three possible outcomes are possible depending on the sign of the radicand.

- Underdamped vibration if $\left(\frac{c}{2m}\right)^2 - \frac{k}{m} < 0 \Longrightarrow \zeta < 1$
- Critically damped vibration if $\left(\frac{c}{2m}\right)^2 - \frac{k}{m} = 0 \Longrightarrow \zeta = 1$
- Overdamped vibration if $\left(\frac{c}{2m}\right)^2 - \frac{k}{m} > 0 \Longrightarrow \zeta > 1$

The only system that actually vibrates is the underdamped one, being it the most common.

3.1.2.1 Underdamped vibration

In this case, $\zeta < 1$, therefore the solutions from Equation 16 can be rewritten as:

$$s_{1,2} = -\zeta\omega_n \pm \omega_n\sqrt{\zeta^2 - 1} = -\zeta\omega_n \pm i\omega_n\sqrt{1 - \zeta^2} = -\zeta\omega_n \pm i\omega_d \tag{17}$$

Where:

$$\omega_d \text{ is the damped natural frequency} \quad \omega_d = \omega_n\sqrt{1 - \zeta^2}$$

In a similar way as the one explained in section 3.1.1, by using the solutions proposed in Equation 17, and replacing them in Equation 13a, the following is obtained.

$$x(t) = X_1 e^{(-\zeta\omega_n + \omega_d i)t} + X_2 e^{(-\zeta\omega_n - \omega_d i)t} = e^{-\zeta\omega_n t}(X_1 e^{\omega_d i t} + X_2 e^{-\omega_d i t}) \tag{18a}$$

$$\dot{x}(t) = (-\zeta\omega_n + \omega_d i)X_1 e^{(-\zeta\omega_n + \omega_d i)t} + (-\zeta\omega_n - \omega_d i)X_2 e^{(-\zeta\omega_n - \omega_d i)t} \tag{18b}$$

Again, to determine the values of X_1 and X_2 the initial conditions are applied ($t = 0$), both for the position (Equation 18a) and the velocity (Equation 18b). Therefore the following system of equations is worked out.

$$\begin{aligned} x_0 &= X_1 + X_2 \\ \dot{x}_0 &= (-\zeta\omega_n + \omega_d i)X_1 + (-\zeta\omega_n - \omega_d i)X_2 = -\zeta\omega_n(X_1 + X_2) + \omega_d i(X_1 - X_2) \end{aligned} \tag{19}$$

By solving the system of equations presented in Equation 19, the following solutions are obtained

$$\boxed{X_1 = \frac{x_0}{2} - i\frac{\zeta\omega_n x_0 + \dot{x}_0}{2\omega_d} \qquad X_2 = \frac{x_0}{2} + i\frac{\zeta\omega_n x_0 + \dot{x}_0}{2\omega_d}}$$

The values of X_1 and X_2 can be expressed in the exponential form ($X = Ae^{i\beta}$). To do so, first of all the imaginary and real parts of each one have to be identified

$$\mathrm{Re}(X_1) = \frac{x_0}{2} \qquad \mathrm{Im}(X_1) = \frac{\zeta\omega_n x_0 + \dot{x}_0}{-2\omega_d} \tag{20a}$$

$$\mathrm{Re}(X_2) = \frac{x_0}{2} \qquad \mathrm{Im}(X_2) = \frac{\zeta\omega_n x_0 + \dot{x}_0}{2\omega_d} \tag{20b}$$

Then, the values of A and β are worked out as follows

$$A_1 = \sqrt{\frac{(x_0\omega_d)^2 + (\dot{x}_0 + \zeta\omega_n x_0)^2}{4\omega_n^2}} = A \quad \beta_1 = \arctan -\frac{\zeta\omega_n x_0 + \dot{x}_0}{x_0\omega_d} = \beta \tag{21a}$$

$$A_2 = \sqrt{\frac{(x_0\omega_d)^2 + (\dot{x}_0 + \zeta\omega_n x_0)^2}{4\omega_n^2}} = A \quad \beta_2 = \arctan \frac{\zeta\omega_n x_0 + \dot{x}_0}{x_0\omega_d} = -\beta \tag{21b}$$

Therefore, taking into account the trigonometry identities ($\sin[-a] = -\sin a$, $\cos[-a] = \cos a$) and Euler's identity ($e^{\theta i} = \cos\theta + i\sin\theta$), Equation 13a can be rewritten as

$$x = e^{-\zeta\omega_n t}(Ae^{\beta i}e^{\omega_d i t} + Ae^{-\beta i}e^{-\omega_d i t}) = 2Ae^{-\zeta\omega_n t}\cos(\omega_d t + \beta) \tag{22}$$

To finish with, the solution to the free underdamped system is

$$\boxed{x(t) = 2Ae^{-\zeta\omega_n t}\cos\left(\omega_d t + \beta\right)} \tag{23}$$

Where

$$A = \sqrt{\frac{(x_0\omega_d)^2 + (\dot{x}_0 + \zeta\omega_n x_0)^2}{4\omega_d^2}}$$
$$\beta = \arctan -\frac{\zeta\omega_n x_0 + \dot{x}_0}{x_0\omega_d}$$

3.1.2.2 Critically damped vibration

In this case, $\zeta = 1$, therefore Equation 16 only has a unique solution, being it

$$s_{1,2} = -\zeta\omega_n \pm \omega_n\sqrt{\zeta^2 - 1} = -\omega_n \tag{24}$$

Again, by replacing the solution proposed in equation Equation 24 in Equation 13a and Equation 13b, the following is obtained

$$x(t) = X_1 e^{-\omega_n t} + X_2 e^{-\omega_n t} \tag{25a}$$
$$\dot{x}(t) = -\omega_n X_1 e^{-\omega_n t} - \omega_n X_2 e^{-\omega_n t} \tag{25b}$$

However, this solution implies that the initial velocity ($\dot{x}_0$) must be different from 0. Actually, the initial velocity can be different than 0, therefore an alternative solution is proposed, which has the following shape

$$x(t) = te^{-\omega_n t} \tag{26a}$$
$$\dot{x}(t) = e^{-\omega_n t} - \omega_n te^{-\omega_n t} = e^{-\omega_n t}(1 - \omega_n t) \tag{26b}$$
$$\ddot{x}(t) = -\omega_n e^{-\omega_n t}(1 - \omega_n t) - \omega_n e^{-\omega_n t} = e^{-\omega_n t}(\omega_n^2 t - 2\omega_n) \tag{26c}$$

Which also satisfy the equation of motion asociated to a free damped system (Equation 14). Therefore, the solution of this problem must be a combination of both of them $e^{-\omega_n t}$ and $te^{-\omega_n t}$

$$x(t) = Ae^{-\omega_n t} + Bte^{-\omega_n t} = (A + Bt)e^{-\omega_n t} \tag{27a}$$
$$\dot{x}(t) = Be^{-\omega_n t} - \omega_n(A + Bt)e^{-\omega_n t} = (B - B\omega_n t - A\omega_n)e^{-\omega_n t} \tag{27b}$$

To determine the values of A and B, the initial conditions ($t = 0$) are applied

$$\begin{aligned} x_0 &= A \\ \dot{x}_0 &= B - A\omega_n \end{aligned} \tag{28}$$

Therefore:

$$\boxed{A = x_0 \qquad B = \dot{x}_0 + x_0\omega_n}$$

To finish with, the solution to the critically damped system is

$$\boxed{x(t) = (A + Bt)e^{-\omega_n t}} \tag{29}$$

Where

$$A = x_0$$
$$B = \dot{x}_0 + x_0\omega_n$$

3.1.2.3 Overdamped vibration

In this case, $\zeta < 1$, therefore Equation 15 yields two real solutions:

$$s_{1,2} = -\zeta\omega_n \pm \omega_n\sqrt{\zeta^2 - 1} \tag{30}$$

Again, by replacing the solution proposed in equation Equation 30 in Equation 13a and Equation 13b, the following is obtained:

$$x(t) = X_1 e^{(-\zeta\omega_n + \omega_n\sqrt{\zeta^2-1})t} + X_2 e^{(-\zeta\omega_n - \omega_n\sqrt{\zeta^2-1})t} = e^{-\zeta\omega_n t}(X_1 e^{\omega_n t\sqrt{\zeta^2-1}} + X_2 e^{-\omega_n t\sqrt{\zeta^2-1}}) \tag{31a}$$
$$\dot{x}(t) = (-\zeta\omega_n + \omega_n\sqrt{\zeta^2 - 1})X_1 e^{(-\zeta\omega_n + \omega_n\sqrt{\zeta^2-1})t} + (-\zeta\omega_n - \omega_n\sqrt{\zeta^2 - 1})X_2 e^{(-\zeta\omega_n - \omega_n\sqrt{\zeta^2-1})t} \tag{31b}$$

To determine the values of X_1 and X_2, the initial conditions are applied

$$\begin{aligned} x_0 &= X_1 + X_2 \\ \dot{x}_0 &= -\zeta\omega_n(X_1 + X_2) + \omega_n\sqrt{\zeta^2 - 1}(X_1 - X_2) \end{aligned} \tag{32}$$

By solving the previous system of equations, the following values are obtained:

$$\boxed{X_1 = \frac{\dot{x}_0 + (\zeta + \sqrt{\zeta^2 - 1})\omega_n x_0}{2\omega_n\sqrt{\zeta^2 - 1}} \qquad X_2 = \frac{-\dot{x}_0 - (\zeta - \sqrt{\zeta^2 - 1})\omega_n x_0}{2\omega_n\sqrt{\zeta^2 - 1}}}$$

To sum up, the solution to the overdamped system is

$$\boxed{x(t) = e^{-\zeta\omega_n t}(X_1 e^{\omega_n t\sqrt{\zeta^2-1}} + X_2 e^{-\omega_n t\sqrt{\zeta^2-1}})} \tag{33}$$

Where

$$X_1 = \frac{\dot{x}_0 + (\zeta + \sqrt{\zeta^2 - 1})\omega_n x_0}{2\omega_n\sqrt{\zeta^2 - 1}}$$
$$X_2 = \frac{-\dot{x}_0 - (\zeta - \sqrt{\zeta^2 - 1})\omega_n x_0}{2\omega_n\sqrt{\zeta^2 - 1}}$$

3.1.3 Case 3: Forced (harmonic force) damped vibration

The equation of motion that describes the conditions in Figure 8c is as follows

$$m\ddot{x} = -c\dot{x} - kx + f \tag{34}$$

Being F an harmonic force with the shape of $f = F\cos\omega_f t = Fe^{i\omega_f t}$

Using an harmonic solution with the form

$$x(t) = Xe^{(\omega t+\delta)i} \tag{35a}$$
$$\dot{x}(t) = X\omega i e^{(\omega t+\delta)i} \tag{35b}$$
$$\ddot{x}(t) = -X\omega^2 e^{(\omega t+\delta)i} \tag{35c}$$

By replacing Equation 35a, Equation 35b and Equation 35c into the equation of motion (Equation 34) the following is obtained (considering $\omega = \omega_f$, as the force will ultimately drive the oscillator)

$$Xe^{(\omega t+\delta)i}(-m\omega^2 + i\omega c + k) = Fe^{i\omega_f t} \Longrightarrow X(-\omega_f^2 + i2\zeta\omega_n\omega_f c + \omega_n^2) = \frac{F}{m}e^{-i\delta} = \frac{F}{m}(\cos(-\delta) + i\sin(-\delta)) \tag{36}$$

Gathering the real and imaginary parts of the RHS and the LHS of Equation 36, the following is obtained

$$\begin{aligned} X(\omega_n^2 - \omega_f^2) &= \frac{F}{m}\cos\delta \\ 2\zeta X\omega_n\omega_f &= -\frac{F}{m}\sin\delta \end{aligned} \tag{37}$$

By squaring both equations, and adding them, the following is obtained, from which the value of X is worked out. Moreover, by dividing both equations the value of δ is also found.

$$X^2\left[(\omega_n^2 - \omega_f^2)^2 + 4\zeta^2\omega_n^2\omega_f^2\right] = \left(\frac{F}{m}\right)^2 \Longrightarrow \boxed{X = \frac{F}{m\sqrt{(\omega_n^2 - \omega_f^2)^2 + 4\zeta^2\omega_n^2\omega_f^2}}}$$

$$\frac{2\zeta X\omega_n}{X(\omega_n^2 - \omega_f^2)} = \frac{\sin\delta}{\cos\delta} \Longrightarrow \boxed{\delta = \arctan\frac{-2\zeta\omega_n\omega_f}{\omega_n^2 - \omega_f^2}}$$

However, this solution is only valid during the steady state. At $t = 0$, the mass behaviour will be different than this, which we call the transient state. To study the transient state, the homogeneous solution of the differential equation must be also included. This solution will depend on which kind of damped system we have (underdamped, overdamped or critically damped). In the following section, we are going to focus on the underdamped situation.

3.1.3.1 Underdamped

In this case, by taking into account the solution proposed in paragraph 3.1.2.1, the following is obtained

$$x(t) = X\cos(\omega_f t + \delta) + Be^{-\zeta\omega_n t}\cos(\omega_d t + \beta) \tag{38a}$$
$$\dot{x}(t) = -\omega_f X\sin(\omega_f t + \delta) - \zeta\omega_n Be^{-\zeta\omega_n t}\cos(\omega_d t + \beta) - \omega_d Be^{-\zeta\omega_n t}\sin(\omega_d t + \beta) \tag{38b}$$

To determine the values of B and β, the initial conditons ($t = 0$) are applied

$$\begin{aligned} x_0 &= X\cos(\delta) + B\cos(\beta) \\ \dot{x}_0 &= -\omega_f X\sin(\delta) - \zeta\omega_n B\cos(\beta) - \omega_d B\sin(\beta) \end{aligned} \tag{39}$$

Therefore:

$$\boxed{\beta = \arctan \frac{1}{\omega_d}\left(\frac{\dot{x}_0 + \omega_f X \sin(\delta)}{X\cos(\delta) - x_0} - \zeta\omega_n\right) \quad B = \frac{x_0 - X\cos(\delta)}{\cos(\beta)}}$$

To sum up, the time response of a driven underdamped system is

$$\boxed{x(t) = X\cos(\omega_f t + \delta) + Be^{-\zeta\omega_n t}\cos(\omega_d t + \beta)} \tag{40}$$

Where

$$\begin{aligned}
X &= \frac{F/m}{\sqrt{(\omega_n^2 - \omega_f^2)^2 + 4\zeta^2\omega_n^2\omega_f^2}} \\
\delta &= \arctan\frac{-2\zeta\omega_n\omega_f}{\omega_n^2 - \omega_f^2} \\
\beta &= \arctan\frac{1}{\omega_d}\left(\frac{\dot{x}_0 + \omega_f X\sin(\delta)}{X\cos(\delta) - x_0} - \zeta\omega_n\right) \\
B &= \frac{x_0 - X\cos(\delta)}{\cos(\beta)}
\end{aligned}$$

3.2 Time integration

A 4^{th} order Runge-Kutta [16] method is used to work out the time integration, as well as an implicit Newmark method [17][18]. These methods are explained in the following sections.

3.2.1 4^{th} order Runge-Kutta time integration

$$\boxed{\ddot{x} + a\dot{x} + bx = f(t) \Longrightarrow \dot{v} + av + bx = f(t)}$$

By definition:

$$dx = v\ dt$$

$$dv = \dot{v}\ dt = (f(t) - av - bx)\ dt = F(x, v, t)\ dt$$

And this method is based on these parameters:

$$\begin{aligned}
dx_1 &= hv & dv_1 &= hF(x_n, v_n, t_n) \\
dx_2 &= h\left(v + \frac{dv_1}{2}\right) & dv_2 &= hF\left(x_n + \frac{dx_1}{2}, v_n + \frac{dv_1}{2}, t_n + \frac{h}{2}\right) \\
dx_3 &= h\left(v + \frac{dv_2}{2}\right) & dv_3 &= hF\left(x_n + \frac{dx_2}{2}, v_n + \frac{dv_2}{2}, t_n + \frac{h}{2}\right) \\
dx_4 &= h(v + dv_3) & dv_4 &= hF\left(x_n + dx_3, v_n + dv_3, t_n + h\right)
\end{aligned}$$

$$\boxed{dx = \frac{dx_1 + 2dx_2 + 2dx_3 + dx_4}{6} \qquad dv = \frac{dv_1 + 2dv_2 + 2dv_3 + dv_4}{6}}$$

$$\boxed{x(t_n + h) = x(t_n) + dx \qquad v(t_n + h) = v(t_n) + dv}$$

Being h the time step.

3.2.2 Newmark's Implicit method

The equations used in this method are the followings:

$$x_{n+1} = x_n + \dot{x}_n h + \left(\frac{1}{2} - \beta\right)\ddot{x}_n h^2 + \beta \ddot{x}_{n+1} h^2 \tag{41}$$

$$\dot{x}_{n+1} = \dot{x}_n + (1-\gamma)\ddot{x}_n h + \gamma \ddot{x}_{n+1} h \tag{42}$$

$$\ddot{x}_{n+1} = -\frac{1}{m}\left[c\dot{x}_{n+1} + f(x_{n+1}) - F_{n+1}\right] \tag{43}$$

This method is unconditionally stable for $\beta = \frac{1}{4}$ and $\gamma = \frac{1}{2}$ The algorithm to perform Newmark's implicit method is as follows:

i) Take an arbitrary value of $\ddot{x}_{n+1}$.

ii) Work out the values of x_{n+1} and $\dot{x}_{n+1}$ using Equation 41 and Equation 42 respectively.

iii) Calculate the value $\ddot{x}_{n+1}$ using the equation of motion (Equation 43).

iv) Check if the initial value from step **i)** and the value calculated in step **iii)** are the same. If so, the process has finished and the next time step is analyzed. If not, we return to step **i)** but this time the guessed value is the one worked out in step **iii)**.

As it can be seen, to begin the iterations the value of the acceleration at $t = 0$ ($\ddot{x}_0$) must be known. This value can be worked out using Equation 43 with the initial conditions ($x = x_0,\ v = v_0,\ t = 0$).

3.2.3 Error and convergence

To check for proper convergence, different values of h (time steps) will be used in the simulations. Then, the last position value of the system will be compared to the modal solution, calculating the absolute and relative error as follows:

$$\epsilon_{abs} = |x_{t_{end}} - x(t_{end})| \qquad \epsilon_{rel} = \frac{\epsilon_{abs}}{x_{t_{end}}} \cdot 100$$

3.2.4 Case 1: Free undamped vibration

The equation of motion that describes the conditons in Figure 8a is as follows:

$$m\ddot{x} + kx = 0 \Longrightarrow \ddot{x} = -\frac{k}{m}x \Longrightarrow \dot{v} = -\frac{k}{m}x$$

Therefore, our $F(x) = -\frac{k}{m}x$. With the following problem conditions:

$$\boxed{m = 4\ \text{kg},\ k = 100\ \text{N}\,\text{m}^{-1},\ x_0 = 2\ \text{m},\ \dot{x}_0 = 0\ \text{m}\,\text{s}^{-1}}$$

And by using the algorithm from Appendix A.1, the following results are obtained, comparing them with the modal solution in Figure 9.

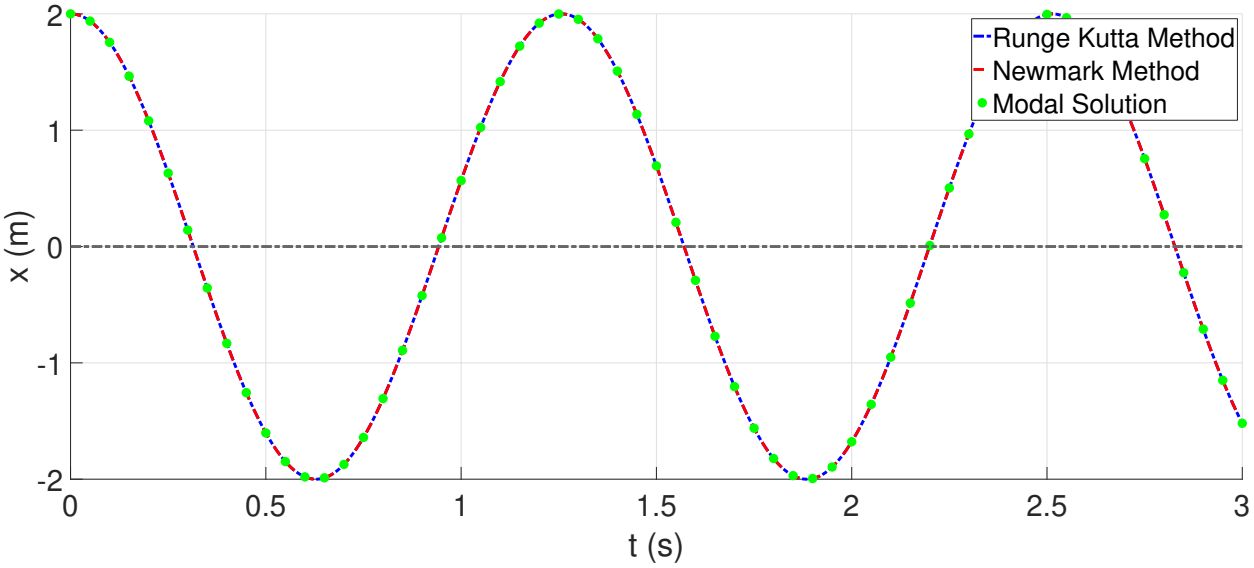

Figure 9: Comparison of the results obtained using Range Kutta and the Newmark Implicit method ($h = 0.00001$ s) with the modal solution

In the following table, the convergence of the method is shown.

Time step, h (s)	Runge Kutta	
	Absolute error (m)	Relative error (%)
0.1	0.01	0.93
0.00001	$3.84 \cdot 10^{-14}$	$3.52 \cdot 10^{-12}$

Time step, h (s)	Newmark	
	Absolute error (m)	Relative error (%)
0.1	1.41	92.47
0.00001	$3.01 \cdot 10^{-4}$	0.02

Table 1: Absolute and relative error

3.2.5 Case 2: Free damped vibration

The equation of motion that describes the conditons in Figure 8b is as follows:

$$m\ddot{x} + c\dot{x} + kx = 0 \Longrightarrow \ddot{x} = -\frac{c}{m}\dot{x} - \frac{k}{m}x \Longrightarrow \dot{v} = -\frac{c}{m}v - \frac{k}{m}x$$

Therefore, our $F(x, v) = -\frac{c}{m}v - \frac{k}{m}x$.

3.2.5.1 Underdamped vibration

With the following problem conditions:

$$\boxed{m = 1\,\text{kg},\ k = 4\,\text{N}\,\text{m}^{-1},\ c = 0.5\,\text{N}\,\text{s}\,\text{m}^{-1},\ x_0 = 2\,\text{m},\ \dot{x}_0 = 0\,\text{m}\,\text{s}^{-1}} \Longrightarrow \zeta = \frac{c}{2\sqrt{km}} = 0.125 < 1$$

And by using the algorithm from Appendix A.2, the following results are obtained, comparing them with the modal solution in Figure 10.

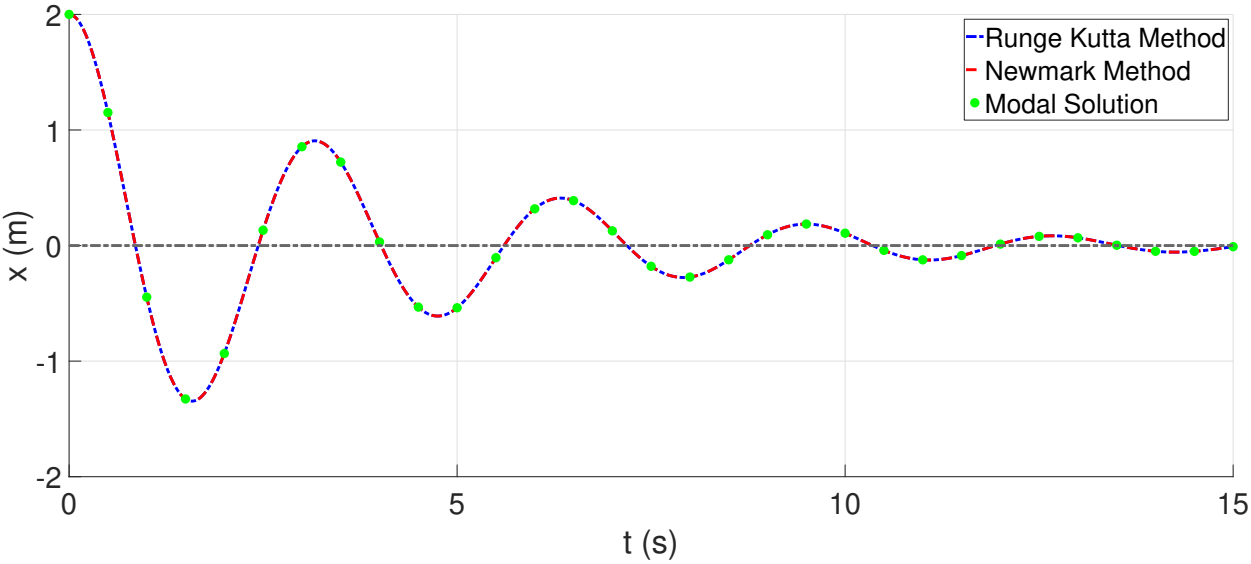

Figure 10: Comparison of the results obtained using Range Kutta and Newmark method ($h = 0.00001$ s) with the modal solution.

In the following table, the convergence of the method is shown.

Time step, h (s)	Runge Kutta	
	Absolute error (m)	Relative error (%)
0.1	$1.87 \cdot 10^{-5}$	0.19
0.00001	$1.23 \cdot 10^{-16}$	$1.27 \cdot 10^{-12}$

Time step, h (s)	Newmark	
	Absolute error (m)	Relative error (%)
0.1	$4.39 \cdot 10^{-4}$	4.54
0.00001	$8.61 \cdot 10^{-7}$	0.01

Table 2: Absolute and relative error

3.2.5.2 Critically damped vibration

With the following problem conditions:

$$\boxed{m = 4\,\text{kg},\ k = 4\,\text{N}\,\text{m}^{-1},\ c = 8\,\text{N}\,\text{s}\,\text{m}^{-1},\ x_0 = 2\,\text{m},\ \dot{x}_0 = 0\,\text{m}\,\text{s}^{-1}} \Longrightarrow \zeta = \frac{c}{2\sqrt{km}} = 1$$

And by using the algorithm from Appendix A.3, the following results are obtained, comparing them with the modal solution in Figure 12.

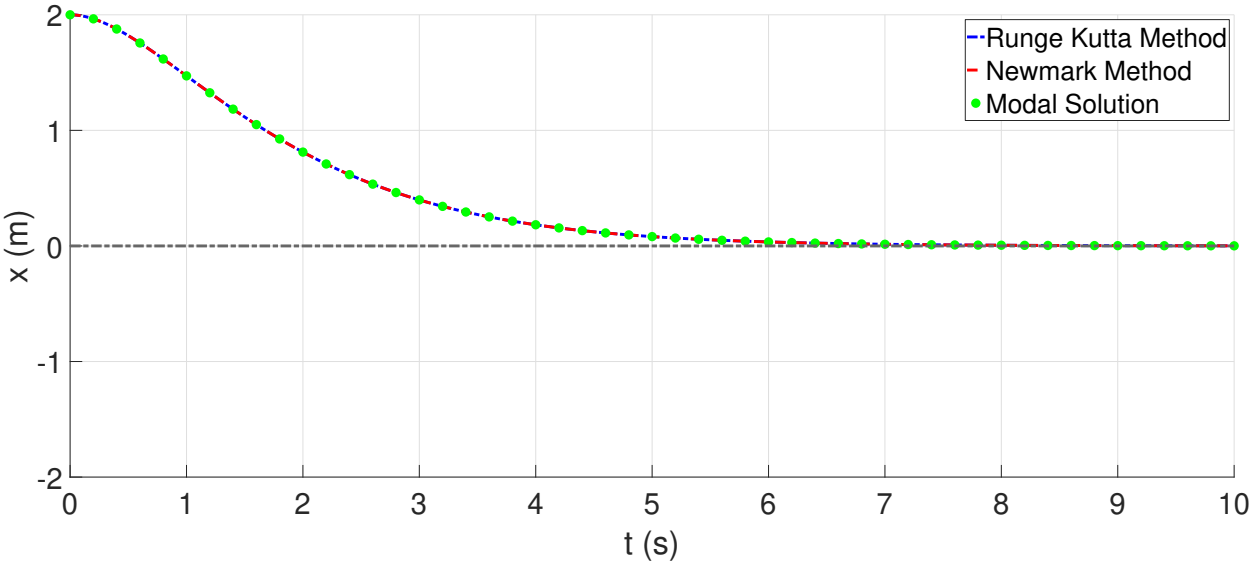

Figure 11: Comparison of the results obtained using Range Kutta and Newmark method ($h = 0.00001$ s) with the modal solution.

In the following table, the convergence of the method is shown.

Time step, h (s)	Runge Kutta	
	Absolute error (m)	Relative error (%)
0.1	$1.86 \cdot 10^{-9}$	$4.87 \cdot 10^{-4}$
0.00001	$1.71 \cdot 10^{-16}$	$1.71 \cdot 10^{-11}$

Time step, h (s)	Newmark	
	Absolute error (m)	Relative error (%)
0.1	$7.67 \cdot 10^{-4}$	76.85
0.00001	$1.98 \cdot 10^{-5}$	1.98

Table 3: Absolute and relative error

3.2.5.3 Overdamped vibration

With the following problem conditions:

$$\boxed{m = 4\ \text{kg},\ k = 4\ \text{N m}^{-1},\ c = 10\ \text{N s m}^{-1},\ x_0 = 2\ \text{m},\ \dot{x}_0 = 0\ \text{m s}^{-1}} \Longrightarrow \zeta = \frac{c}{2\sqrt{km}} = 1.25 > 1$$

And by using the algorithm from Appendix A.4, the following results are obtained, comparing them with the modal solution in Figure 12.

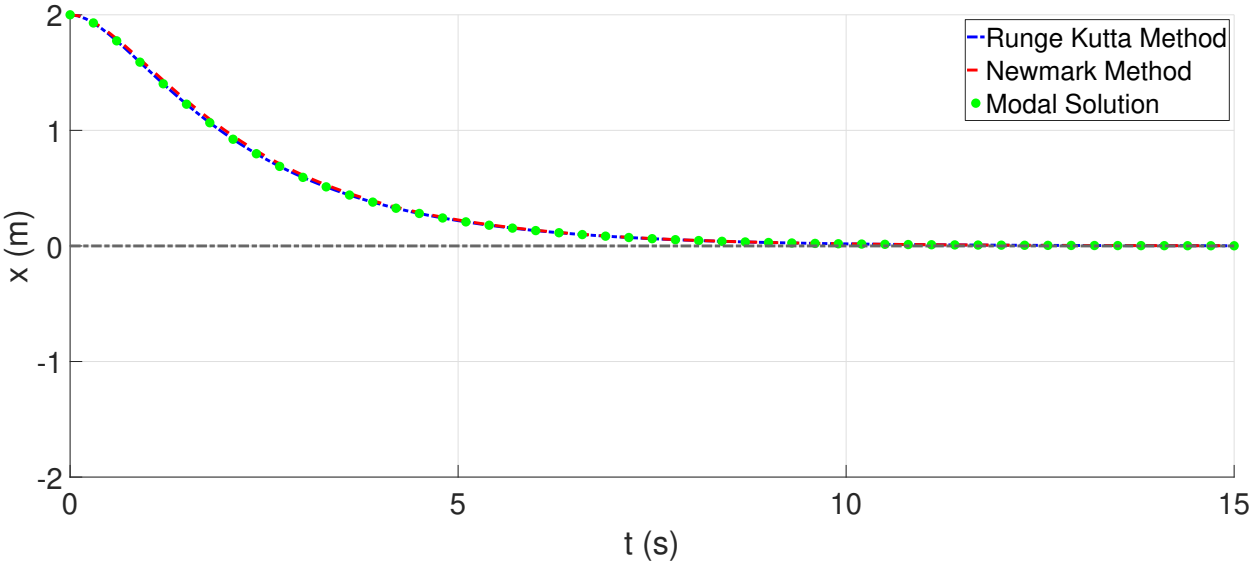

Figure 12: Comparison of the results obtained using Range Kutta and Newmark method ($h = 0.00001$ s) with the modal solution.

In the following table, the convergence of the method is shown.

Time step, h (s)	Runge Kutta	
	Absolute error (m)	Relative error (%)
0.1	$6.01 \cdot 10^{-10}$	$4.07 \cdot 10^{-5}$
0.00001	$5.64 \cdot 10^{-17}$	$3.82 \cdot 10^{-12}$

Time step, h (s)	Newmark	
	Absolute error (m)	Relative error (%)
0.1	$3.17 \cdot 10^{-4}$	21.52
0.00001	$2.49 \cdot 10^{-5}$	1.69

Table 4: Absolute and relative error

3.2.6 Case 3: Forced underdamped vibration

The equation of motion that describes the conditions in Figure 8c is as follows:

$$m\ddot{x} + c\dot{x} + kx = F\cos(\omega_f t) \Longrightarrow \ddot{x} = -\frac{c}{m}\dot{x} - \frac{k}{m}x + \frac{F}{m}\cos(\omega_f t) \Longrightarrow \dot{v} = -\frac{c}{m}v - \frac{k}{m}x + \frac{F}{m}\cos(\omega_f t)$$

Therefore, in this case $F(x, v, t) = -\frac{c}{m}v - \frac{k}{m}x + \frac{F}{m}\cos(\omega_f t)$. With the folowwing problem conditions:

$$m = 1\ \text{kg},\ k = 4\ \text{N m}^{-1},\ c = 0.5\ \text{N s m}^{-1},\ F = 2\ \text{N},\ \omega_f = 1.5\ \text{rad s}^{-1},\ x_0 = 2\ \text{m},\ \dot{x}_0 = 0\ \text{m s}^{-1}$$

And by using the algorithm from Appendix A.5, the following results are obtained, comparing them with the modal solution in Figure 13.

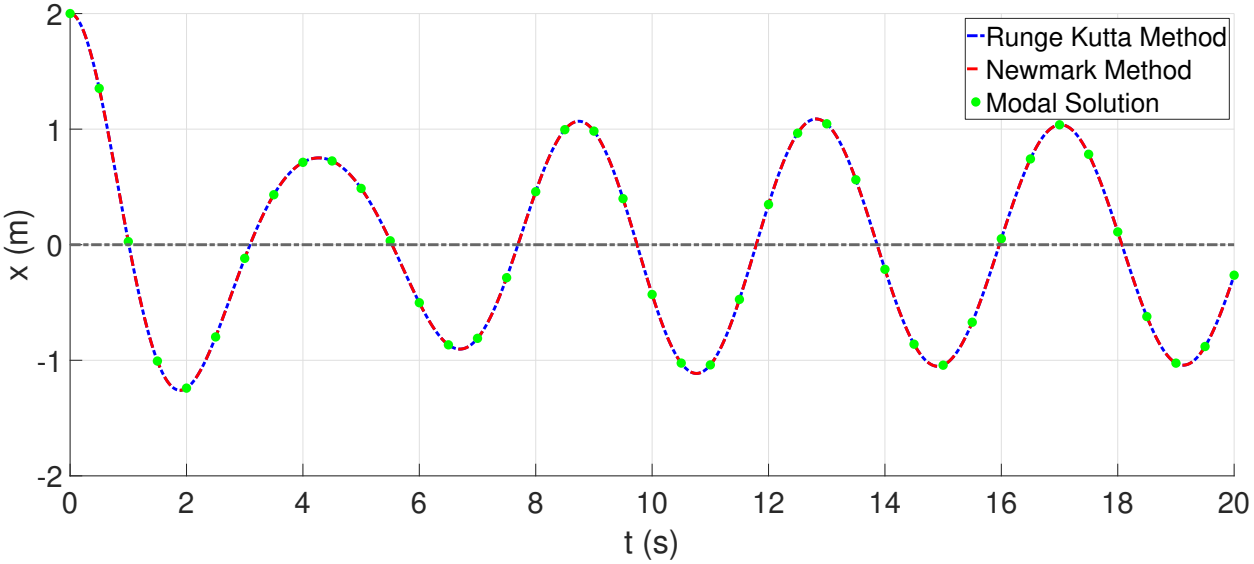

Figure 13: Comparison of the results obtained using Range Kutta and Newmark method ($h = 0.00001$ s) with the modal solution.

In the following table, the convergence of the method is shown.

Time step, h (s)	Runge Kutta	
	Absolute error (m)	Relative error (%)
0.1	$1.22 \cdot 10^{-5}$	0.01
0.00001	$1.82 \cdot 10^{-14}$	$6.91 \cdot 10^{-14}$

Time step, h (s)	Newmark	
	Absolute error (m)	Relative error (%)
0.1	0.2	75.89
0.00001	$1.95 \cdot 10^{-5}$	0.01

Table 5: Absolute and relative error

3.3 Exponential spring analysis

Now a new case will be studied. In this one, the spring will have a non-linear behaviour, in order to verify that the time integrations developed in the previous section properly work, resulting the equation of motion for Figure 8c as follows:

$$m\ddot{x} + c\dot{x} + f(x) = F$$

Where

$$f(x) = f_0\left(1 - e^{-\frac{k}{f_0}x}\right)$$

3.3.1 Time integration

In both methods the time step used is 0.00001 seconds ($h = 0.00001$ s).

To apply the Runge-Kutta method, first of all the $F(x, v, t)$ must be identified. In this case:

$$F(x, v, t) = -\frac{c}{m}v - \frac{f_0}{m}\left(1 - e^{-\frac{k}{f_0}x}\right) + F\cos\left(\omega_f t\right)$$

3.3.1.1 Free damped vibration

Using the algorithm from Appendix A.6, with the following problem conditions:

$$\boxed{m = 1\ \text{kg}\ k = 4\ \text{N}\,\text{m}^{-1}\ c = 0.5\ \text{N}\,\text{s}\,\text{m}^{-1}\ x_0 = 2\ \text{m}\ v_0 = 0\ \text{m}\,\text{s}^{-1}}$$

The results shown below are obtained.

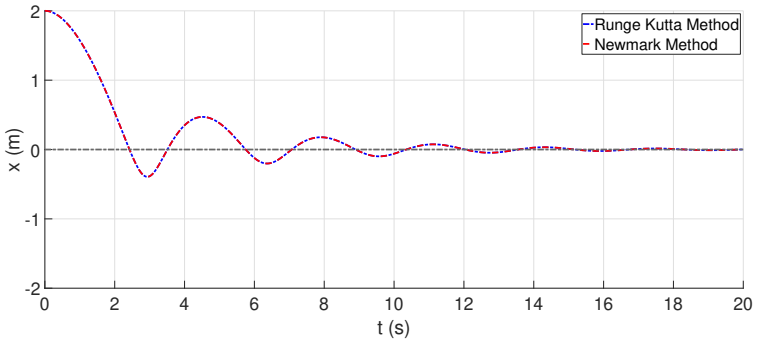

(a) Time response with a non-linear k ($f_0 = 1$ N)

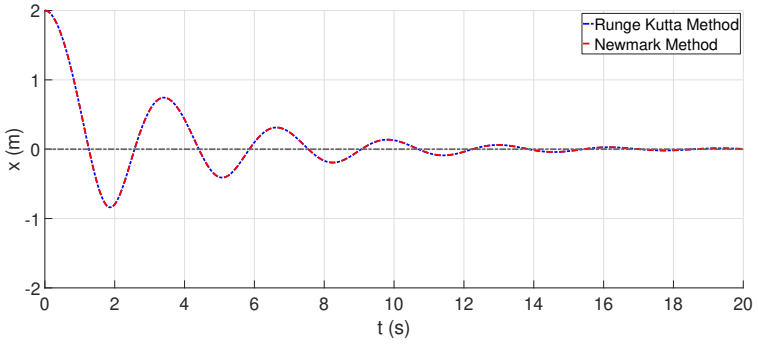

(b) Time response with a non-linear k ($f_0 = 4$ N)

Figure 14: Time response with a non-linear k, both with the Runge-Kutta and the Newmark time integration method

3.3.1.2 Forced damped vibration

Using the algorithm from Appendix A.7, with the following problem conditions:

$$m = 1\ \text{kg}\ k = 4\ \text{N}\,\text{m}^{-1}\ c = 0.5\ \text{N}\,\text{s}\,\text{m}^{-1}\ x_0 = 0\ \text{m}\ v_0 = 0\ \text{m}\,\text{s}^{-1}\ F = 2\ \text{N}\ \omega_F = 1.5\ \text{rad}\,\text{s}^{-1}$$

The results shown below are obtained.

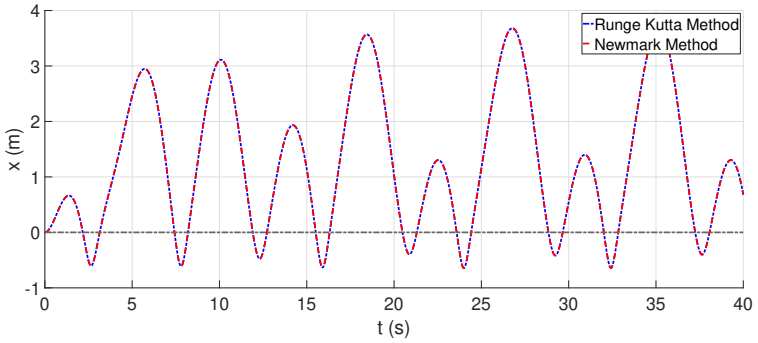

(a) Time response with a non-linear k ($f_0 = 1$ N)

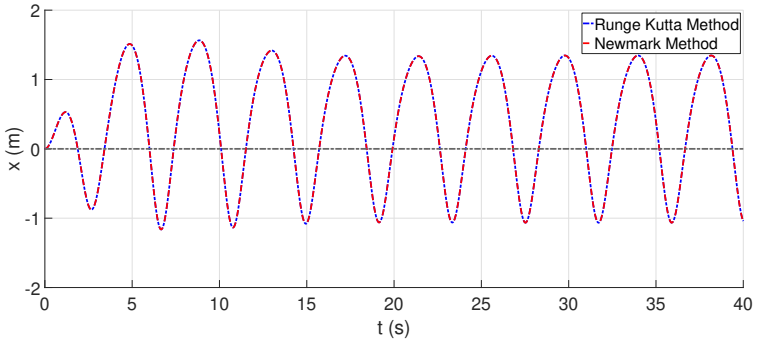

(b) Time response with a non-linear k ($f_0 = 4$ N)

Figure 15: Time response with a non-linear k, both with the Runge-Kutta and the Newmark time integration method

3.4 Controlled force analysis

In this section the spring will have a piecewise linear behaviour as shown in Figure 7, roughly simulating the real behaviour of the snap-through phenomena. The external force will grow at a constant rate (v_F) as shown in Figure 16.

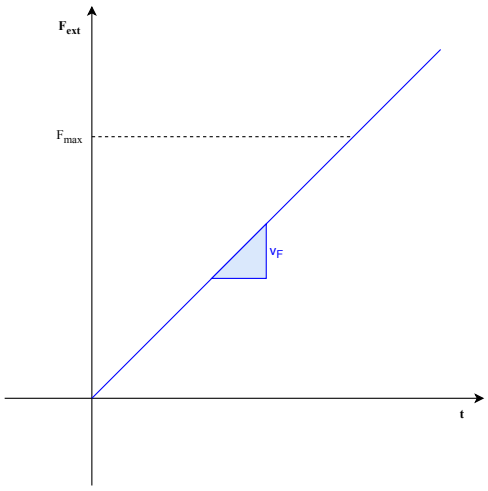

Figure 16: External force application

Additionally, a really small value of v_F must be taken in order to ensure that the problem can be considered a quasi-static one. In this case the period of the system ($T = \sqrt{m/k_0}$) will be used as the critical value, having to be the v_F lower than it. Therefore the equation of motion in this case is as follows:

$$\boxed{m\ddot{x} + c\dot{x} + F_{int}(x) = F_{ext}(t)}$$

3.4.1 Meta-stable behaviour

In this case the minimum value of the internal force (F_{min}) is still positive. Using the following problem values, as well as the *MATLAB* code from Appendix A.8

$$\boxed{m = 1\,\text{kg} \quad k_0 = 4\,\text{N m}^{-1} \quad k_1 = 2\,\text{N m}^{-1} \quad c = 0.5\,\text{N s m}^{-1} \quad F_{max} = 10\,\text{N} \quad F_{min} = 2\,\text{N} \quad v_f = {}^{T}/_{100}}$$

And being the initial conditions $x_0 = 0$ m and $v_0 = 0\,\text{m s}^{-1}$, the following results are obtained

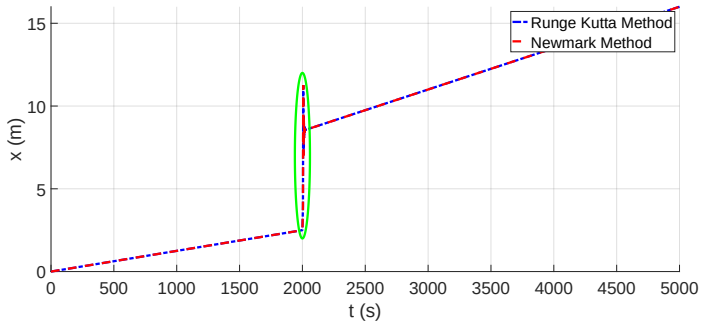

(a) Displacement time response of the mass

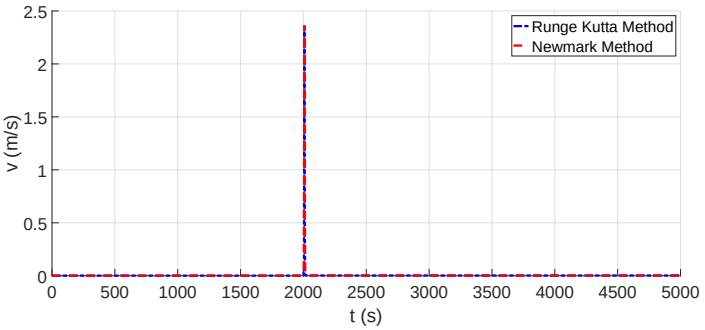

(b) Velocity time response of the mass

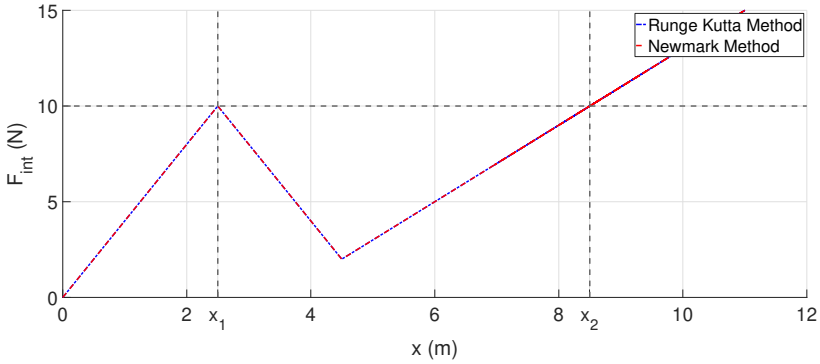

(c) Internal force evolution as a function of the displacement

Figure 17: Behaviour of the system using a piecewise linear spring (meta-stable)

By zooming in the circle drawn on Figure 17a, the following plot is obtained.

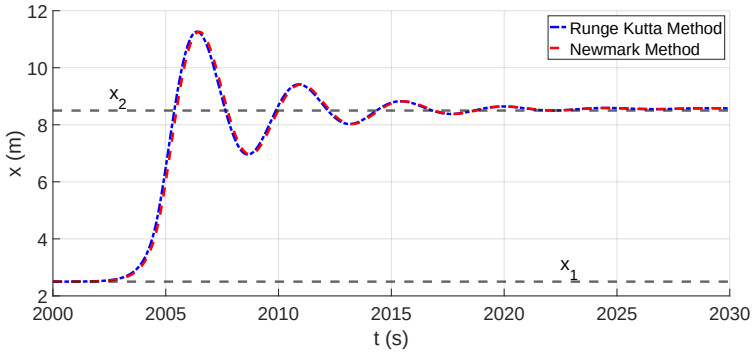

Figure 18: Zoom into the green zone from Figure 17a

Several conclusions can be extracted from these results.

- Both integration methods yield similar results (Figure 18), meaning that the time integration has been properly performed.
- The velocity during all the simulation is negligibly, only spiking when sudden position change takes place.
- The points at which the internal force reaches the established maximum value ($F_{int} = F_{max}$) - which can be seen in Figure 17c, points x_1 and x_2 - are the ones at which the system stabilize before and after the position change, as can be seen in Figure 18

To follow with, several simulations have been performed using different damping values (c), ranging from underdamped to overdamped, including the critically damped value. The code used to perform this sweep analysis is Appendix A.9.

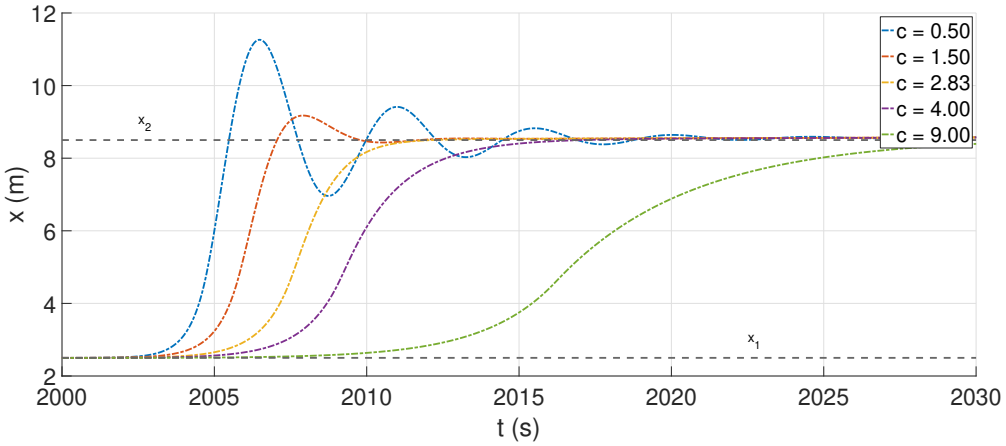

Figure 19: Time integration results using multiple damping ratios (Newmark Method, $h = 0.0001$ s)

As it can be seen in Figure 19, the transition from x_1 to x_2 loses its vibratory behaviour as the damping ratio increases, up to $c = 2.48\ \mathrm{N\,s\,m^{-1}}$, which is the critical value and causes the smoothest switch. From here,

if the value of c is increased the system has an overdamped transition. Let's focus now on the critically damped case. Comparing Figure 17b with Figure 20, it can be seen that while in the former the velocity peak oscillates a little bit, in the later it does not.

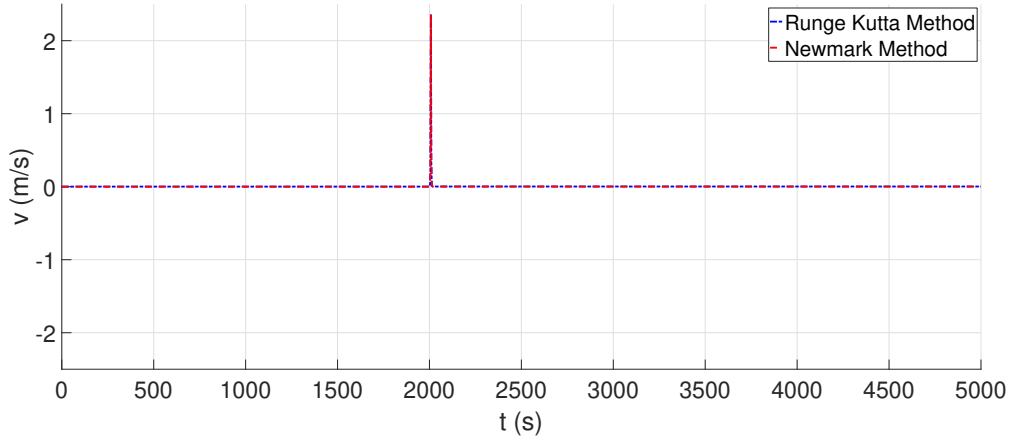

Figure 20: Time evolution of the mass velocity in the critically damped case.

3.4.1.1 Load-unload problem

In this subsection the behaviour of the system will be studied under a whole load-unload cycle. The external force will reach a maximum value and from there it will start decreasing at the same pace that it did during the loading period. The code used to perform this analysis can be found in Appendix A.10.

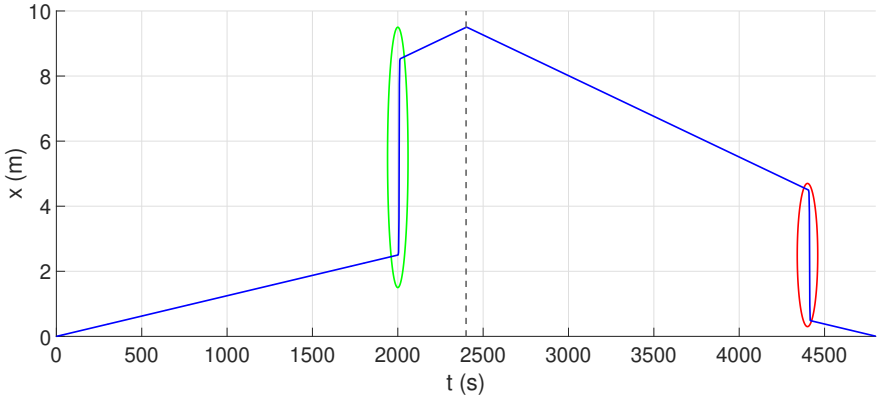

(a) Displacement of the mass under a load-unload situation

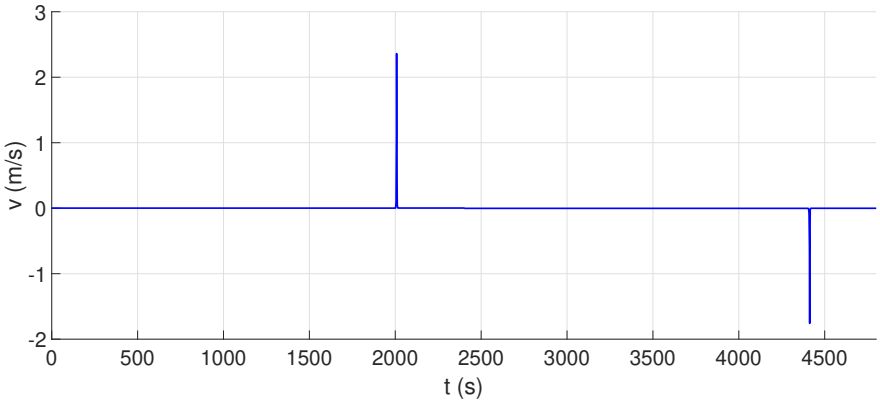

(b) Velocity of the mass under a load-unload situation

Figure 21: Behaviour of the system using a piecewise linear spring under a load-unload problem (Newmark Method,$h = 0.0001$ s)

Figure 21a represents the displacement along all the simulation, growing the external force from $t = 0$ s to $t = 2400$ s, and decreasing from the later point until it reaches 0 again at $t = 48000$ s. As it can be seen, a similar phenomena (circled in red) happens during the unloading process to the one that has been explained in the section above. Let's focus now on these two circles.

First of all there's the loading process (green circle, Figure 21a), depicted below.

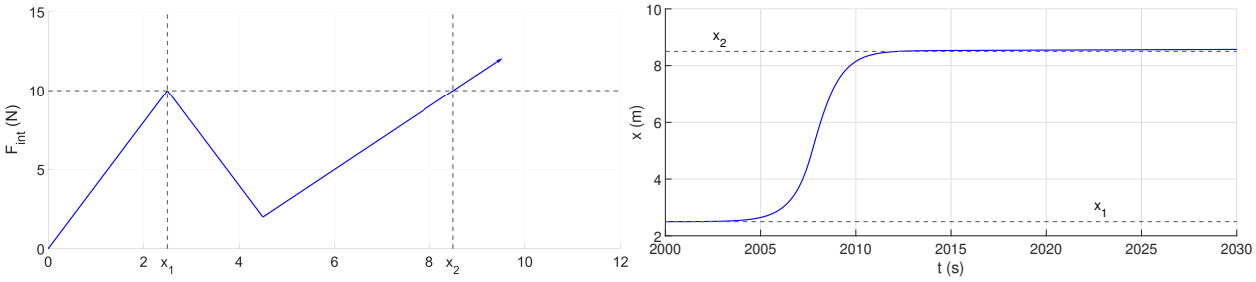

(a) Internal force.

(b) Sudden position change.

Figure 22: Behaviour of the system during the loading process

As it is shown, and has been explained before, the values before and after the sudden position change (x_1 and x_2) coincide with the ones represented in Figure 22a. Secondly, there is the unloading process (red circle, Figure 21a).

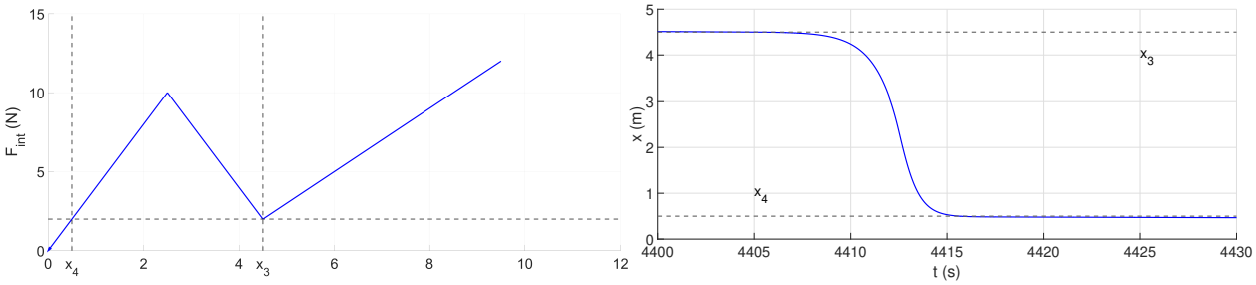

(a) Internal force.

(b) Snap-through phenomena.

Figure 23: Behaviour of the system during the unloading process

A similar phenomena takes place during the unloading process. When the internal force reaches the minimum value (F_{min}) another snap-through takes place. Again, the values before and after the switch (x_3 and x_4, represented in Figure 23b) are the same as the ones at which the internal force value is equal to the minimum one established (Figure 23a).

To finish with, as it can be seen in Figure 21b, the velocity is 0 during all the process, except when the snap-through takes place. In order to smooth both switches the value of the damper has been changed to a critically damped one: during the loading process $c = 2 \cdot \sqrt{mk_1}$ while during the unloading process $c = 2 \cdot \sqrt{mk_0}$. Nonetheless, there isn't much difference between these two as k_1 and k_0 are quite similar.

3.4.1.2 Energy dissipation

Taking the loading-unloading problem explained above as the starting point, an energy analysis is performed in this section. To better represent the energy dissipation during this process, the external force is plotted against the displacement in the following figure.

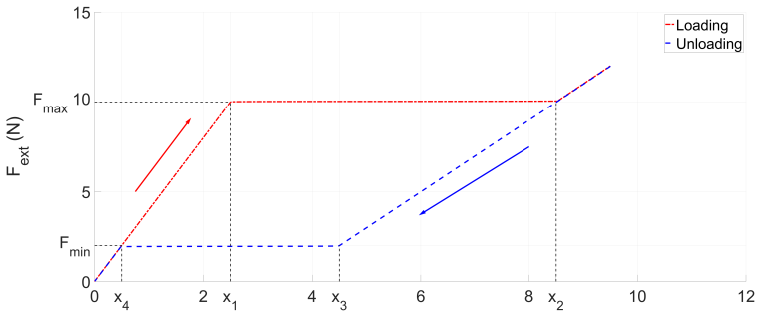

Figure 24: Hysteresis cycle of the system

The area compressed between the loading and unloading curve equals the energy dissipated. This area equals:

$$A = A_1 + A_2 = \frac{(4.5 - 0.5) \cdot (10 - 2)}{2} + \frac{(8.5 - 2.5) \cdot (10 - 2)}{2} = 16\ \text{J} + 24\ \text{J} = 40\ \text{J}$$

This value is related with the damping of the system. To check this relation, the motion equation is taken as starting point, and it is multiplied by the velocity on both sides.

$$m\ddot{x} + c\dot{x} + F_{int}(x) = F_{ext}(t) \longrightarrow m\ddot{x}\dot{x} + c\dot{x}^2 + F_{int}(x)\dot{x} = F_{ext}(t)\dot{x}$$

By replacing the new terms using energy values (U kinetic energy, E_d dissipated energy, E_{int} internal energy, E_{ext} external energy) the following is obtained:

$$\frac{dU}{dt} + \frac{dE_d}{dt} + \frac{dE_{int}}{dt} = \frac{dE_{ext}}{dt}$$

From which the values of the energy itself can be calculated:

- $U = \int_{t_1}^{t_2} \frac{dU}{dt}\, dt = U(t_2) - U(t_1)$
- $E_d = \int_{t_1}^{t_2} \frac{dE_d}{dt}\, dt = \int_{t_1}^{t_2} c\dot{x}^2\, dt$
- $E_{int} = \int_{t_1}^{t_2} \frac{dE_{int}}{dt}\, dt = \int_{t_1}^{t_2} F_{int}(x)\dot{x}\, dt$
- $E_{ext} = \int_{t_1}^{t_2} \frac{dE_{ext}}{dt}\, dt = \int_{t_1}^{t_2} F_{int}(x)\dot{x}\, dt$

Whenever this integrals have to be performed, the trapezoidal method is used.

3.4.1.2.1 Loading

To energetically analyze the loading process, the 4 integrals showed above will be calculated between $t = 0$ and $t = t_{lim}$, being t_{lim} the time instance at which the external force reaches 12 N. The values of the internal and external energy can be worked out by calculating the area below the graphics $F_{int}(x)$ (red one) and $F_{ext}(x)$ (blue one) respectively (Figure 25).

$$A_{int} = 59.5 \text{ J} \qquad A_{ext} = 83.5 \text{ J} \qquad A_d = A_{ext} - A_{int} = 24 \text{ J}$$

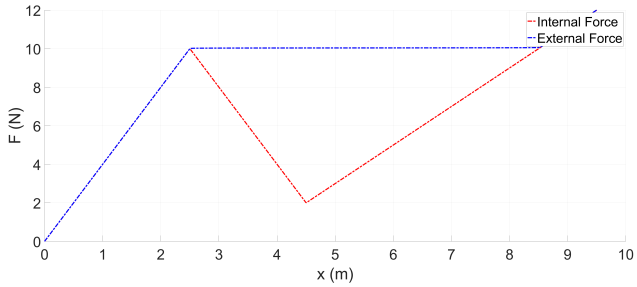

Figure 25: External and internal force plotted against the displacement

- $U = \int_0^{t_{lim}} \frac{dU}{dt}\, dt = U(t_{lim}) - U(0) \longrightarrow \boxed{U = 0 \text{ J}}$
- $E_d = \int_0^{t_{lim}} \frac{dE_d}{dt}\, dt = \int_0^{t_{lim}} c\dot{x}^2\, dt \longrightarrow \boxed{E_d = 24.01 \text{ J}}$
- $E_{int} = \int_0^{t_{lim}} \frac{dE_{int}}{dt}\, dt = \int_0^{t_{lim}} F_{int}(x)\dot{x}\, dt \longrightarrow \boxed{E_{int} = 59.5 \text{ J}}$
- $E_{ext} = \int_0^{t_{lim}} \frac{dE_{ext}}{dt}\, dt = \int_0^{t_{lim}} F_{ext}(x)\dot{x}\, dt \longrightarrow \boxed{E_{ext} = 83.51 \text{ J}}$

As it can be seen, the values obtained using the trapezoidal rule are quite similar to the ones expected (the internal energy perfectly matches the area value calculated above, and the external energy only differs by 0.01 J). Moreover, the energy dissipated - E_d - coincides with the value expected - A_d - (being the relative error 0.04 %).

3.4.1.2.2 Unloading

To energetically analyze the unloading process, the 4 integrals showed above will be calculated between $t = t_{lim}$ and $t = t_{end}$, being t_{lim} the time instance at which the external force reaches 12 N, and t_{end} the instance at which the external force reaches 0 N. The values of the internal and external energy can be worked out by calculating the area below the graphics $F_{int}(x)$ (red one) and $F_{ext}(x)$ (blue one) respectively (Figure 26).

$$A_{int} = 59.5 \text{ J} \qquad A_{ext} = 43.5 \text{ J} \qquad A_d = A_{int} - A_{ext} = 16 \text{ J}$$

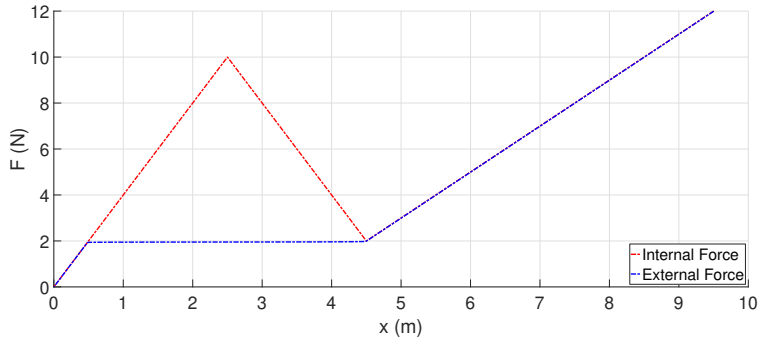

Figure 26: External and internal force plotted against the displacement

- $U = \int_{t_{lim}}^{t_{end}} \frac{dU}{dt}\, dt = U(t_{lim}) - U(0) \longrightarrow \boxed{U = 0 \text{ J}}$
- $E_d = \int_{t_{lim}}^{t_{end}} \frac{dE_d}{dt}\, dt = \int_{t_{lim}}^{t_{end}} c\dot{x}^2\, dt \longrightarrow \boxed{E_d = 15.99 \text{ J}}$
- $E_{int} = \int_{t_{lim}}^{t_{end}} \frac{dE_{int}}{dt}\, dt = \int_{t_{lim}}^{t_{end}} F_{int}(x)\dot{x}\, dt \longrightarrow \boxed{E_{int} = 59.5 \text{ J}}$
- $E_{ext} = \int_{t_{lim}}^{t_{end}} \frac{dE_{ext}}{dt}\, dt = \int_{t_{lim}}^{t_{end}} F_{ext}(x)\dot{x}\, dt \longrightarrow \boxed{E_{ext} = 43.51 \text{ J}}$

As it can be seen, the values obtained using the trapezoidal rule are quite similar to the ones expected (the internal energy perfectly matches the area value calculated above, and the external energy only differs by 0.01 J). Furthermore, the energy dissipated - E_d - coincides with the value expected - A_d - (being the relative error 0.04 %).

	Area Value	Numerical Integration Value
E_d Loading	16	15.99
E_d Unloading	24	24.01
E_d Total	40	40

Table 6: Summary of the energy analysis performed

3.4.1.3 Load-stop problem

In this situation, once the external force reaches its maximum value (12 N), rather than decreasing at a steady pace, it will plummet down to 0 N. To perform the analysis the *MATLAB* code from Appendix A.11. The following results are obtained

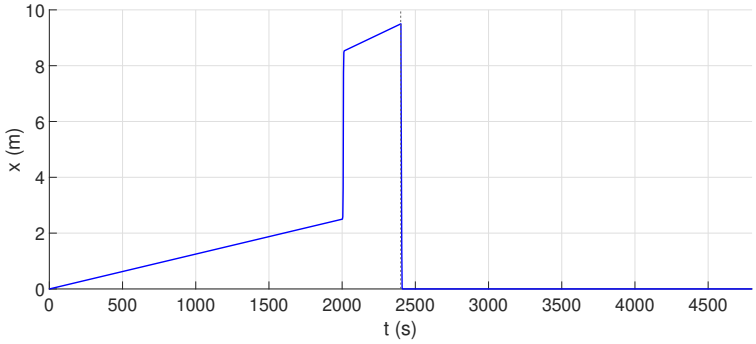

(a) Displacement of the mass along the time domain

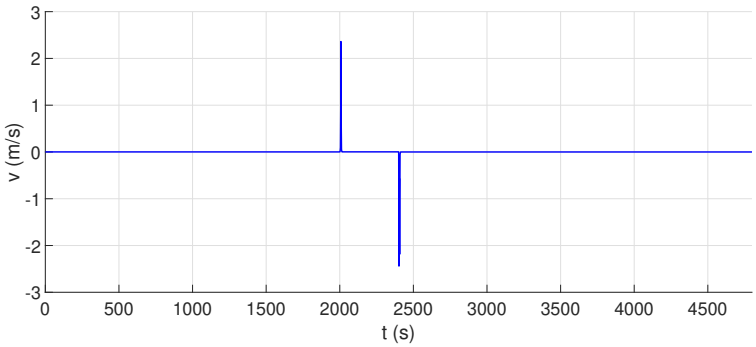

(b) Velocity of the mass along the time domain

Figure 27: Behaviour of a meta-stable system under loading-unloading conditions

As it is shown in Figure 27a, as soon as the external force suddenly decreases to 0, the system quickly goes back to its initial position.

3.4.2 Bi-stable behaviour

A bi-stable behaviour better represents the snap-through phenomena [19], as it only has two stable positions. In this case the minimum value of the internal force (F_{min}) is negative. Using the following problem values as well as the *MATLAB* code from Appendix A.8.

$$m = 1\ \text{kg} \quad k_0 = 4\ \text{N m}^{-1} \quad k_1 = 2\ \text{N m}^{-1} \quad c = 2.48\ \text{N s m}^{-1} \quad F_{max} = 10\ \text{N} \quad F_{min} = -2\ \text{N} \quad v_f = T/100$$

And being the initial conditions $x_0 = 0$ m and $v_0 = 0\ \text{m s}^{-1}$, the following results are obtained

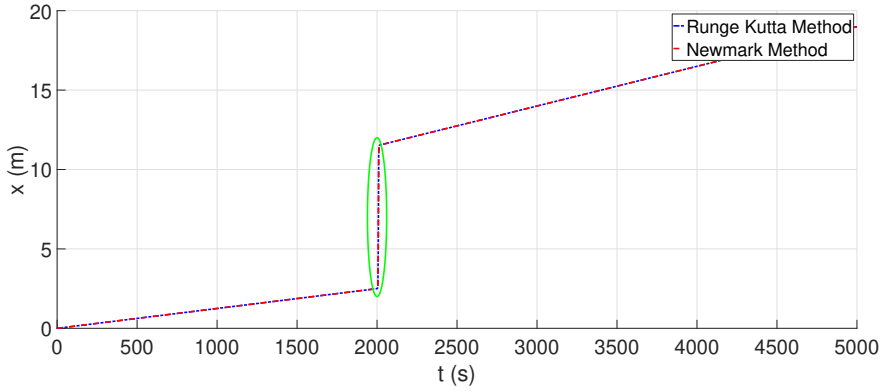

(a) Displacement time response of the mass

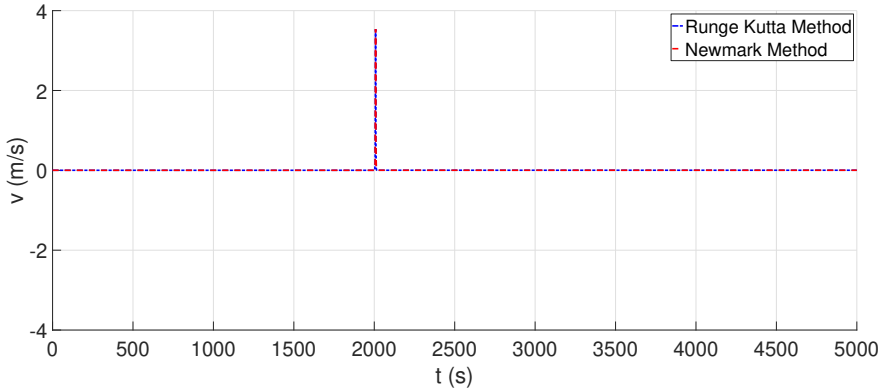

(b) Velocity time response of the mass

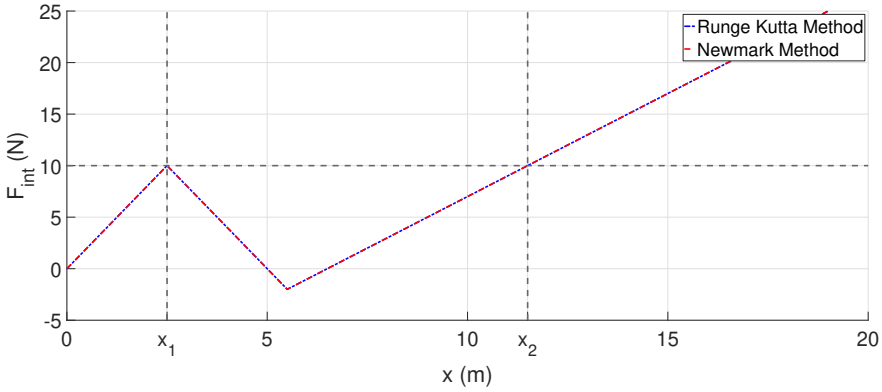

(c) Internal force evolution as a function of the displacement

Figure 28: Behaviour of the system using a piecewise linear spring (bi-stable)

Zooming in Figure 28a reveals the following

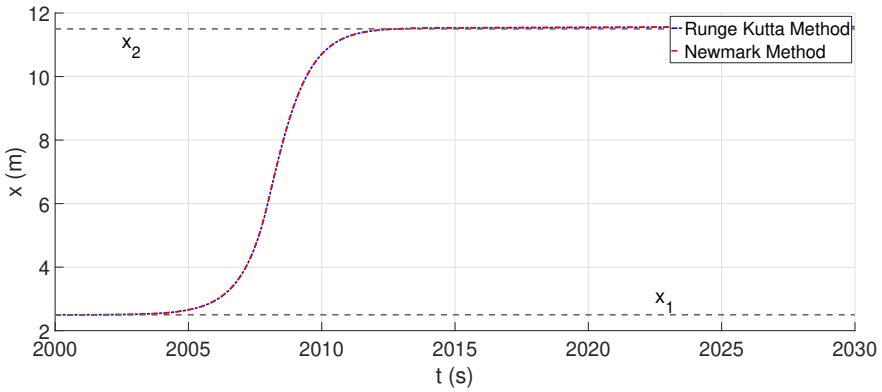

Figure 29: Zoom into the green zone from Figure 28a

As it can be seen from Figure 28 and Figure 29, the behaviour of the bi-stable system is quite similar to the meta-stable explained before, with some minor differences due to the lower minimum internal force value (F_{min}).

However, until this point only the loading process has been studied (which yields identical results to the meta-stable explained before). The following situation to study is the load-stop problem.

3.4.2.1 Load-Stop problem

As in the meta-stable case, the external force will reach a maximum value, and from there it will drop down to 0 N. The *MATLAB* code used to perform the analysis can be found in Appendix A.12. The following results are obtained

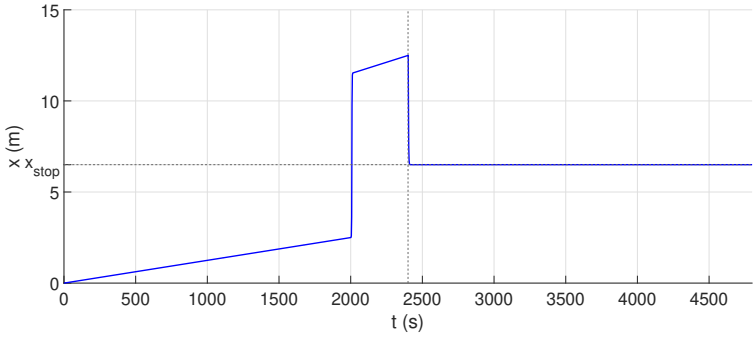

(a) Displacement of the mass along the time domain

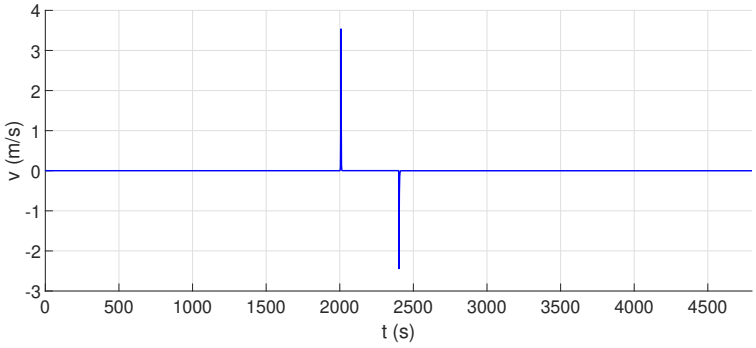

(b) Velocity of the mass along the time domain

Figure 30: Behaviour of the bi-stable system under a loading-stop enviroment

As it can be seen in Figure 30a, rather than plummeting down to the initial position as the meta-stable system did (Figure 27a), in this case the system stabilizes arround a certain value (x_{stop}) after the external force is instantly withdrawn. To better understand this ocurrence, an analysis of the internal force evolution along all the process must be performed.

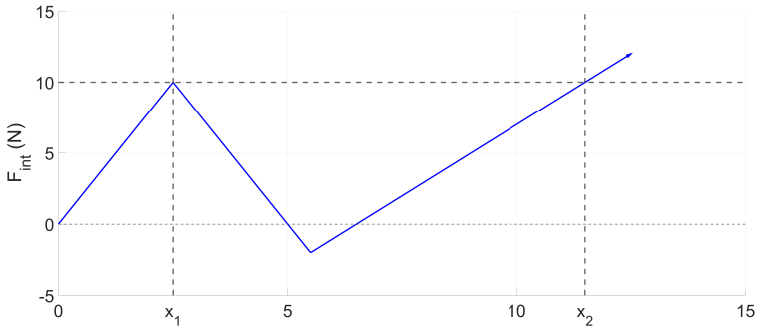

(a) Loading process (before the force removal)

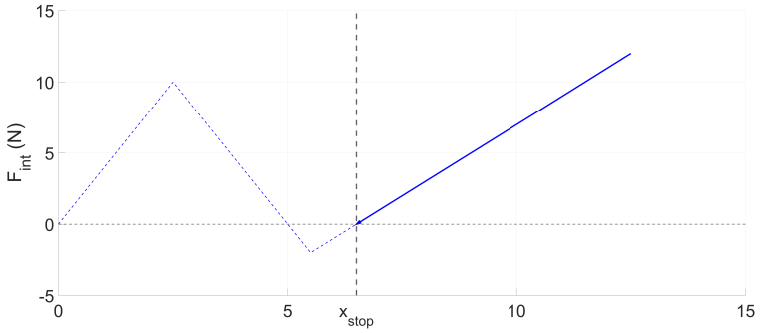

(b) Unloading process (after the force removal)

Figure 31: Internal force evolution of the bi-stable system under a loading-stop process

As it can be seen in Figure 31a, the loading process is completely normal and matches what has been studied until this point. When it comes to the unloading process however, rather than following the trend that has been seen before (Figure 23a), the internal force stalls as it reaches 0 N. It can be concluded that in this case, after the force removal, the system stores certain amount of energy.

3.5 Controlled displacement analysis

Now that the controlled force displacement analysis has been performed (and the snap-through phenomena has been shown), the controlled displacement analysis will be studied, in order to display the snap-back behaviour. In this case the analysis will be further extended to multiple consequent piecewise linear springs, but to begin with, a one piecewise spring system will be studied. This system is shown in Figure 32.

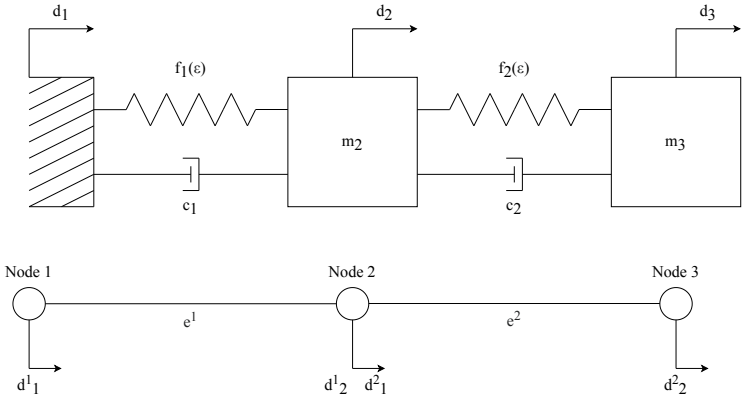

Figure 32: Two spring system

In Figure 32 stands for the relative distance between the two nodes of one element (thus being it the spring elongation, $\epsilon^e = d_2^e - d_1^e$). Besides, f_1 and f_2 are the spring functions, having the second one a linear behaviour ($f_2(\epsilon) = k_2\epsilon$) and the first one the piecewise linear behaviour explained in the previous section (Equation 1). This equation, adapted to the new terminology, yields Equation 44.

$$f_1(\epsilon) = \begin{cases} k_0 \cdot \epsilon & 0 \leq \epsilon < \epsilon_{max} \\ f_{max} - k_0 \cdot (\epsilon - \epsilon_{max}) & \epsilon_{max} \leq \epsilon < \epsilon_{min} \\ f_{min} + k_1 \cdot (\epsilon - \epsilon_{min}) & \epsilon_{min} \leq \epsilon \end{cases} \tag{44}$$

Analyzing the situation depicted Figure 32, the following motion equations are obtained, for m_1, m_2 and m_3 respectively

$$m_1\ddot{d_1} - c_1(\dot{d_2} - \dot{d_1}) - f_1(\epsilon^1) = 0$$

$$m_2\ddot{d_2} + c_1(\dot{d_2} - \dot{d_1}) - c_2(\dot{d_3} - \dot{d_2}) + f_1(\epsilon^1) - f_2(\epsilon^2) = 0$$

$$m_3\ddot{d_3} + c_2(\dot{d_3} - \dot{d_2}) + f_2(\epsilon^2) = 0$$

Where

$$\epsilon^1 = d_2^1 - d_1^1 = d_2 - d_1 \qquad e^2 = d_2^2 - d_1^2 = d_3 - d_2$$

Therefore the equations can be rewritten as:

$$m_1\ddot{d}_1 - c_1(\dot{d}_2 - \dot{d}_1) - f_1(d_2 - d_1) = 0$$

$$m_2\ddot{d}_2 + c_1(\dot{d}_2 - \dot{d}_1) - c_2(\dot{d}_3 - \dot{d}_2) - f_2(d_3 - d_2) + f_1(d_2 - d_1) = 0$$

$$m_3\ddot{d}_3 + c_2(\dot{d}_3 - \dot{d}_2) + f_2(d_3 - d_2) = 0$$

To perform the analysis of the system, the equations of motion are written using the following matrix notation

$$\boldsymbol{M}\ddot{\boldsymbol{d}} + \boldsymbol{C}\dot{\boldsymbol{d}} + \boldsymbol{F}^{int} = \boldsymbol{F}^{ext} + \boldsymbol{R}$$

$$\begin{bmatrix} m_1 & 0 & 0 \\ 0 & m_2 & 0 \\ 0 & 0 & m_3 \end{bmatrix} \begin{bmatrix} \ddot{d}_1 \\ \ddot{d}_2 \\ \ddot{d}_3 \end{bmatrix} + \begin{bmatrix} c_1 & -c_1 & 0 \\ -c_1 & c_1 + c_2 & -c_2 \\ 0 & -c_2 & c_2 \end{bmatrix} \begin{bmatrix} \dot{d}_1 \\ \dot{d}_2 \\ \dot{d}_3 \end{bmatrix} + \begin{bmatrix} -f_1(d_2 - d_1) \\ f_1(d_2 - d_1) - f_2(d_3 - d_2) \\ f_2(d_3 - d_2) \end{bmatrix} = \boldsymbol{F}^{ext} + \boldsymbol{R}$$

First of all, before starting the analysis, the restricted (R) and free nodes (L) must be identified. To begin with, the first node does not move, therefore its displacement, velocity and acceleration are always 0 ($d_1 = \dot{d}_1 = \ddot{d}_1 = 0$). Besides, in this case rather than applying an external force as it has been done before (imposed force analysis), the displacement of the third node will be prescribed (imposed displacement analysis), thus why the external forces in the matrix equation depicted below are 0. The displacement of the third mass will be linear and its velocity will be very low and constant (therefore, $\dot{d}_3 \simeq 0$ and $\ddot{d}_3 = 0$). Therefore, by reorganizing the matrix equation (taking into account which nodes are free and which are restricted), the following is obtained

$$\begin{bmatrix} m_1 & 0 & 0 \\ 0 & m_3 & 0 \\ 0 & 0 & m_2 \end{bmatrix} \begin{bmatrix} \ddot{d}_1 = 0 \\ \ddot{d}_3 = 0 \\ \ddot{d}_2 \end{bmatrix} + \begin{bmatrix} c_1 & 0 & -c_1 \\ 0 & c_2 & -c_2 \\ -c_1 & -c_2 & c_1 + c_2 \end{bmatrix} \begin{bmatrix} \dot{d}_1 = 0 \\ \dot{d}_3 \\ \dot{d}_2 \end{bmatrix} + \begin{bmatrix} -f_1(d_2) \\ f_2(d_3 - d_2) \\ f_1(d_2) - f_2(d_3 - d_2) \end{bmatrix} = \begin{bmatrix} 0 \\ 0 \\ 0 \end{bmatrix} + \begin{bmatrix} R_1 \\ R_3 \\ 0 \end{bmatrix}$$

To work out the displacement of the second mass (d_2), its equation of motion will be used.

$$m_2\ddot{d_2} = c_2(\dot{d_3} - \dot{d_2}) - c_1\dot{d_2} + f_2(d_3 - d_2) - f_1(d_2)$$

To work out the reactions of the first and third mass, once d_2 has been worked out, their equations of motion will be used.

$$R_1 = -f_1(d_2) \qquad R_3 = f_2(d_3 - d_2) + c_2(\dot{d_3} - \dot{d_2})$$

First of all, a really low value of velocity has been imposed to make the analysis as accurate as possible.

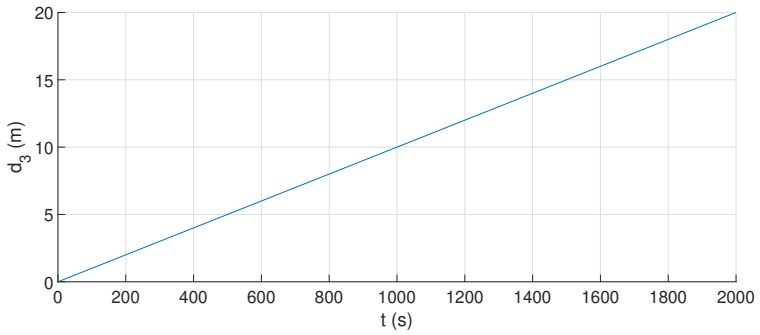

Figure 33: Imposed displacement of the third mass along the time ($v_3 = 10^{-2}\ \mathrm{m\,s^{-1}}$)

3.5.1 Meta-stable behaviour

By using the code from Appendix A.13, sweeping through multiple values of the first element spring stiffness (k_1), the following is obtained:

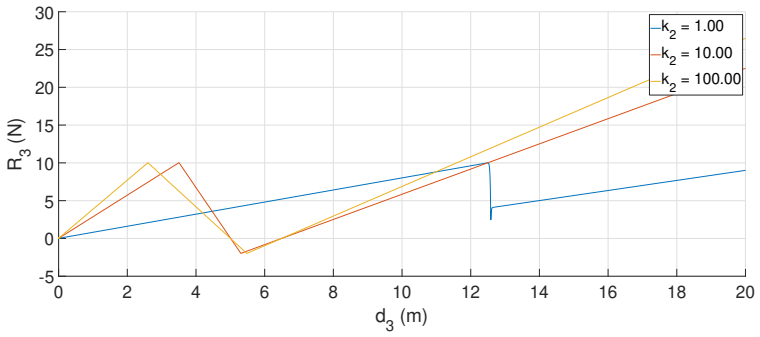

(a) Reaction of the third mass as a function of its displacement

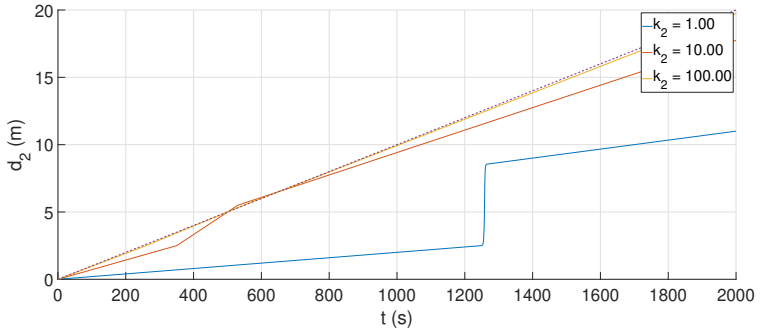

(b) Displacement of the second node along the time domain

Figure 34: Results of the 2 spring system for various values of k_2

As it can be seen from Figure 34a, as we increase the second element spring constant (k_2), reaction change becomes less brusque, as the transition stretches along the time. Moreover, as Figure 34b shows, the second mass movement follows the third mass as the spring constant increases.

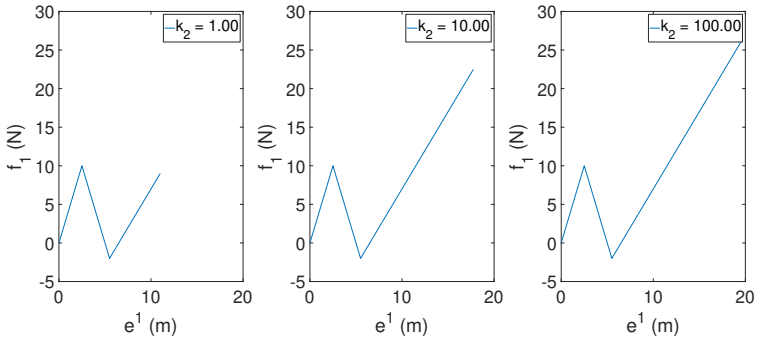

(a) Tracking of the first spring force as function of the spring elongation

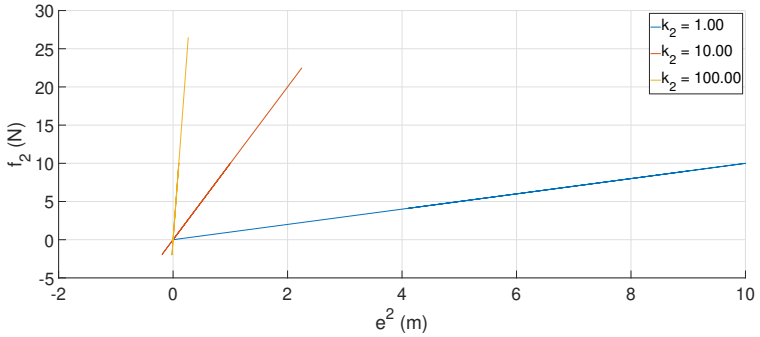

(b) Tracking of the second spring force as function of the spring elongation

Figure 35: Validation of the behaviour imposed on the springs

As it can be seen in Figure 35b and Figure 35a, the spring force follows the prescribed behaviour in both cases (piecewise linear in the first one and linear in the second one).

As it has been seen in Figure 34b, the snap-back phenomena only takes place for a small value of k_2 ($k_2 = 1\,\mathrm{N\,m^{-1}}$). Below, a study of smaller values of k_2 is performed.

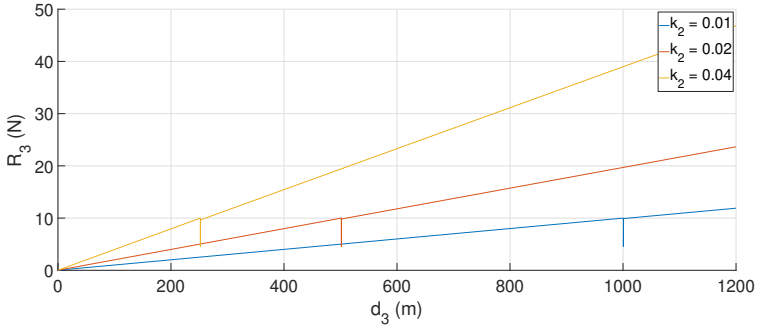

Figure 36: Reaction of the third mass as a function of its displacement

At first sight, Figure 36 does not show anything relevant, so the plot is going to be zoomed in the sudden change of the reaction force for each spring value.

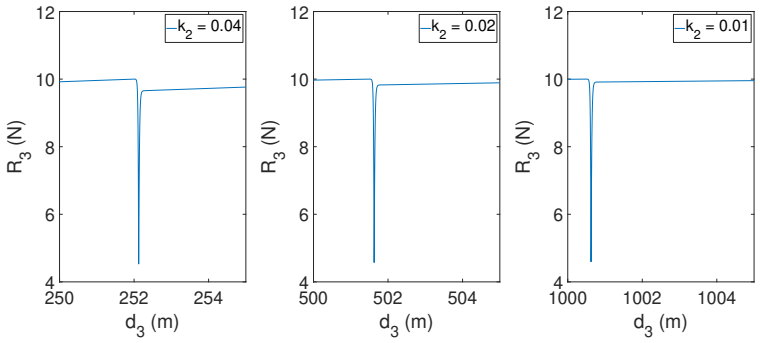

(a) Zoomed in reaction force (1)

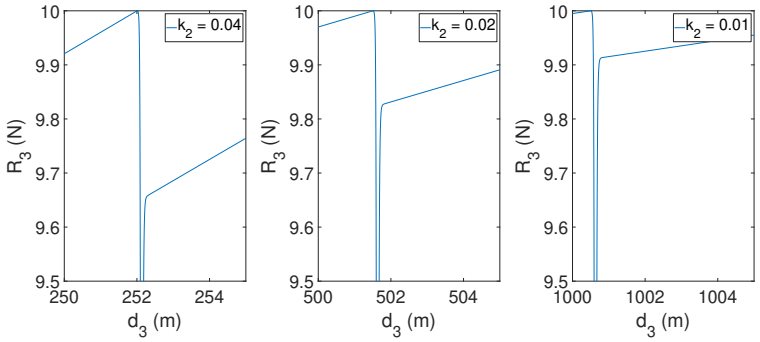

(b) Zoomed in reaction force (2)

Figure 37: Zoom in Figure 36

First of all, as it can be seen in Figure 37b, despite falling down to the same value, as k_2 decreases, the value of the reaction force after the snap-back increases, getting closer to the one it was (10 N) before the snap-back. Secondly, as Figure 37a shows, in all three cases the reaction force dips to the same value. To better explain this, the equation of motion of the third mass (used to calculate R_3) is recovered below

$$R_3 = c_2(v_3 - v_2) + f_2$$

The reaction force is essentially the internal force plus the damping force of c_2. As v_3 is very low (its value has been established as 0.01 $\mathrm{m\,s^{-1}}$, most of its contribution comes from the second mass velocity (v_2). Figure 38 shows that in all three cases, when the snap-back phenomena takes place, the mass velocity is the same despite the value of k_2.

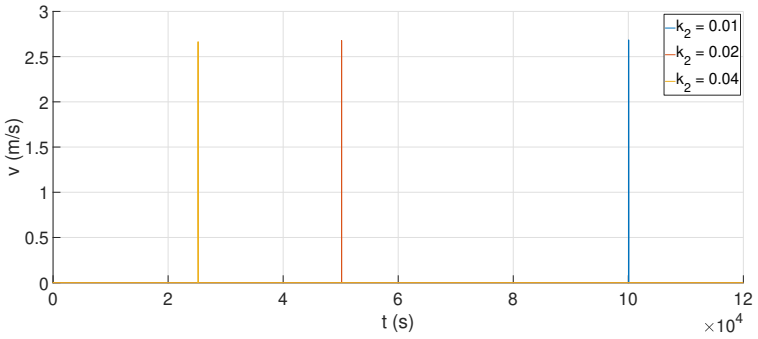

Figure 38: Velocity of the second mass along time

3.5.1.1 Energy analysis

Again, as in the controlled forced case, an energy analysis is performed. Another load-unload process as depicted in Figure 39 will be analysed. In this case the problem conditions are shown below:

$$m_1 = m_2 = m_3 = 1\,\text{kg} \quad c_1 = c_2 = 1\,\text{N s m}^{-1} \quad v_3 = 0.01\,\text{m s}^{-1} \quad k_0 = 4\,\text{N m}^{-1} \quad k_1 = \frac{k_0}{2} \quad k_2 = \frac{k_1}{2}$$

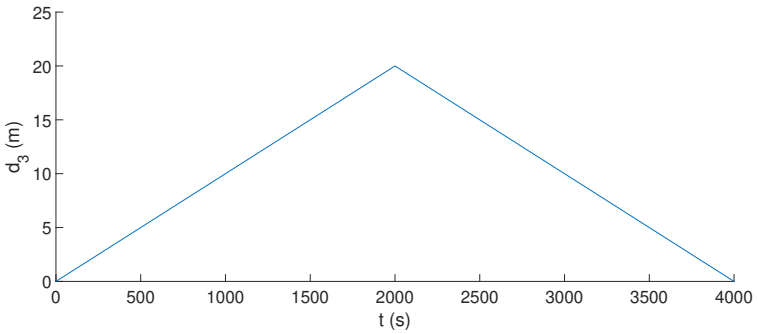

Figure 39: Displacement of the third mass along time.

First of all the equations of motion for the three masses are shown below in a matrix form

$$\boldsymbol{M}\ddot{\boldsymbol{d}} + \boldsymbol{C}\dot{\boldsymbol{d}} + \boldsymbol{F}^{int} = \boldsymbol{R}$$

$$\begin{bmatrix} m_1 & 0 & 0 \\ 0 & m_2 & 0 \\ 0 & 0 & m_3 \end{bmatrix} \begin{bmatrix} \ddot{d}_1 = 0 \\ \ddot{d}_2 \\ \ddot{d}_3 = 0 \end{bmatrix} + \begin{bmatrix} c_1 & -c_1 & 0 \\ -c_1 & c_1 + c_2 & -c_2 \\ 0 & -c_2 & c_2 \end{bmatrix} \begin{bmatrix} \dot{d}_1 = 0 \\ \dot{d}_2 \\ \dot{d}_3 \end{bmatrix} + \begin{bmatrix} -f_1(d_2) \\ f_1(d_2) - f_2(d_3 - d_2) \\ f_2(d_3 - d_2) \end{bmatrix} = \begin{bmatrix} R_1 \\ 0 \\ R_3 \end{bmatrix}$$

As it has been done before, both sides of the equation are multiplied by the velocity vector

$$\dot{\boldsymbol{d}}^T \boldsymbol{M}\ddot{\boldsymbol{d}} + \dot{\boldsymbol{d}}^T \boldsymbol{C}\dot{\boldsymbol{d}} + \dot{\boldsymbol{d}}^T \boldsymbol{F}^{int} = \dot{\boldsymbol{d}}^T \boldsymbol{R}$$

By replacing the new terms using energy values (U kinetic energy, E_d dissipated energy, E_{int} internal energy, E_R reaction energy), the equation above can be rewritten as

$$\frac{dU}{dt} + \frac{dE_d}{dt} + \frac{dE_{int}}{dt} = \frac{dE_{ext}}{dt}$$

Taking into account that $\dot{d}_1 = \ddot{d}_1 = \ddot{d}_3 = 0$, the remaining equations can be rewritten as:

$$\frac{dU}{dt} = \begin{bmatrix} \dot{d}_2 & \dot{d}_3 \end{bmatrix} \begin{bmatrix} m_2 & 0 \\ 0 & m_3 \end{bmatrix} \begin{bmatrix} \ddot{d}_2 \\ 0 \end{bmatrix} = \dot{d}_2 m_2 \ddot{d}_2$$

$$\frac{dE_d}{dt} = \begin{bmatrix} \dot{d}_2 & \dot{d}_3 \end{bmatrix} \begin{bmatrix} c_1 + c_2 & -c_2 \\ -c_2 & c_2 \end{bmatrix} \begin{bmatrix} \dot{d}_2 \\ \dot{d}_3 \end{bmatrix} = (c_1 + c_2)\dot{d}_2^2 - c_2\dot{d}_3\dot{d}_2 + c_2\dot{d}_3(\dot{d}_3 - \dot{d}_2)$$

$$\frac{dE_{int}}{dt} = \begin{bmatrix} \dot{d}_2 & \dot{d}_3 \end{bmatrix} \begin{bmatrix} f_1(d_2) - f_2(d_3 - d_2) \\ f_2(d_3 - d_2) \end{bmatrix} = \dot{d}_2 f_1(d_2) + (\dot{d}_3 - \dot{d}_2) f_2(d_3 - d_2)$$

$$\frac{dE_{ext}}{dt} = \begin{bmatrix} \dot{d}_2 & \dot{d}_3 \end{bmatrix} \begin{bmatrix} 0 \\ R_3 \end{bmatrix} = R_3 \dot{d}_3$$

Integrating each term, their respective energies can be obtained.

- $U = \int_{t_1}^{t_2} \frac{dU}{dt}\, dt$
- $E_d = \int_{t_1}^{t_2} \frac{dE_d}{dt}\, dt$
- $E_{int} = \int_{t_1}^{t_2} \frac{dE_{int}}{dt}\, dt$
- $E_{ext} = \int_{t_1}^{t_2} \frac{dE_R}{dt}\, dt$

As it has been done before, the trapezoidal rule is applied in order to compute the necessary integrals.

By plotting the reaction of the third mass (R_3) against its displacement, the following is obtained.

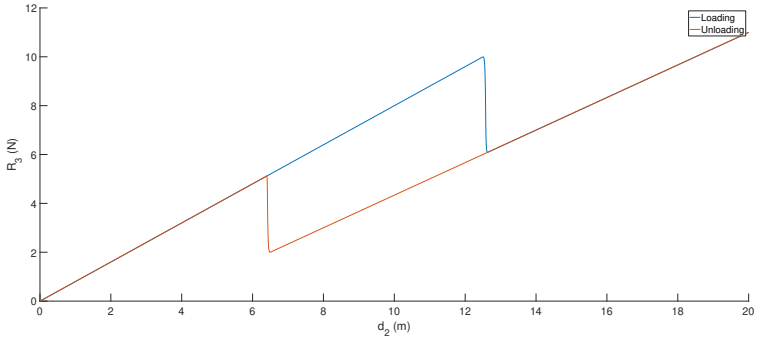

Figure 40: Load-unload process under a controlled displacement analysis

As it can be seen, the loading and unloading process follow different paths. Below, each energy value (U, E_d, E_{int}, E_{ext}) is computed for both the loading, and unloading process. After that, the total energy dissipated will be compared to the area enclosed in Figure 40

First of all, the loading process

- $U = \int_{t_{lim}}^{t_{end}} \frac{dU}{dt}\, dt \longrightarrow \boxed{U = 0 \text{ J}}$
- $E_d = \int_{t_{lim}}^{t_{end}} \frac{dE_d}{dt}\, dt \longrightarrow \boxed{E_d = 12.47 \text{ J}}$
- $E_{int} = \int_{t_{lim}}^{t_{end}} \frac{dE_{int}}{dt}\, dt \longrightarrow \boxed{E_{int} = 114.25 \text{ J}}$
- $E_{ext} = \int_{t_{lim}}^{t_{end}} \frac{dE_{ext}}{dt}\, dt \longrightarrow \boxed{E_{ext} = 126.72 \text{ J}}$

And secondly, the unloading process

- $U = \int_{t_{lim}}^{t_{end}} \frac{dU}{dt}\, dt \longrightarrow \boxed{U = 0 \text{ J}}$
- $E_d = \int_{t_{lim}}^{t_{end}} \frac{dE_d}{dt}\, dt \longrightarrow \boxed{E_d = 10 \text{ J}}$
- $E_{int} = \int_{t_{lim}}^{t_{end}} \frac{dE_{int}}{dt}\, dt \longrightarrow \boxed{E_{int} = -114.25 \text{ J}}$
- $E_{ext} = \int_{t_{lim}}^{t_{end}} \frac{dE_{ext}}{dt}\, dt \longrightarrow \boxed{E_{ext} = -104.25 \text{ J}}$

In both cases the following equation is satisfied

$$U + E_{int} + E_d = E_{ext}$$

Finally, the enclosed area from Figure 40 is calculated using the *trapz* function from *MATLAB*, and the following value is obtained

$$\text{Enclosed area} = 22.47 \text{ J}$$

Which, indeed, matches with the sum of the loading/unloading values of E_d

$$E_d^{loading} + E_d^{unloading} = 12.47 + 10 = 22.47 \text{ J}$$

3.6 System of N springs

The same analysis performed before will be done to analyse a system made up of N, having the first springs the piecewise behaviour explained during the project (f_1 to f_{N-1}), and the last one (N) having a typical linear behaviour (f_N).

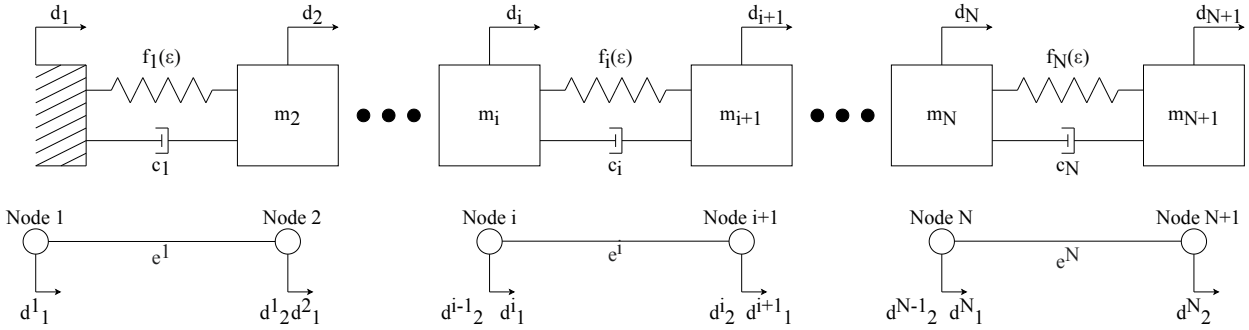

Figure 41: N spring system

In this case, assuming that $c_1 = c_2 = c_i = c_N = c$ and $m_1 = m_2 = m_i = m_N = m$, the equations of motion can be written as follows

$$\begin{aligned} i = 1 &\longrightarrow m\ddot{d}_i - c(\dot{d}_{i+1} - \dot{d}_i) - f_i(\epsilon^i) = R_i \\ i = [2, ..., N-1] &\longrightarrow m\ddot{d}_i + c(\dot{d}_i - \dot{d}_{i-1}) - c(\dot{d}_{i+1} - \dot{d}_i) + f_{i-1}(\epsilon^{i-1}) - f_i(\epsilon^i) = 0 \\ i = N+1 &\longrightarrow m\ddot{d}_i + c(\dot{d}_i - \dot{d}_{i-1}) + f_{i-1}(\epsilon^{i-1}) = R_i \end{aligned}$$

Taking into account that $\ddot{d}_1 = \dot{d}_1 = d_1 = \ddot{d}_{N+1} = 0$, the equations can be further simplified into

$$\begin{aligned} i = 1 &\longrightarrow c\dot{d}_{i+1} - f_i(\epsilon^i) = R_i \\ i = [2, ..., N-1] &\longrightarrow m\ddot{d}_i + c(\dot{d}_i - \dot{d}_{i-1}) - c(\dot{d}_{i+1} - \dot{d}_i) + f_{i-1}(\epsilon^{i-1}) - f_i(\epsilon^i) = 0 \\ i = N+1 &\longrightarrow c(\dot{d}_i - \dot{d}_{i-1}) + f_{i-1}(\epsilon^{i-1}) = R_i \end{aligned}$$

The code from Appendix A.15 is used to perform the study.

3.6.1 Meta-stable behaviour

By performing two analysis with $N = 4 + 1$ and $N = 8 + 1$ springs, with the following problem conditions

$$m = 1\,\text{kg} \quad c = 1\,\text{N}\,\text{s}\,\text{m}^{-1} \quad v_{N+1} = 0.01\,\text{m}\,\text{s}^{-1} \quad k_0 = 4\,\text{N}\,\text{m}^{-1} \quad k_1 = \frac{k_0}{2} \quad k_N = \frac{k_1}{20} \quad F_{max} = 10\,\text{N} \quad F_{max} = 2\,\text{N}$$

The graphics below are obtained

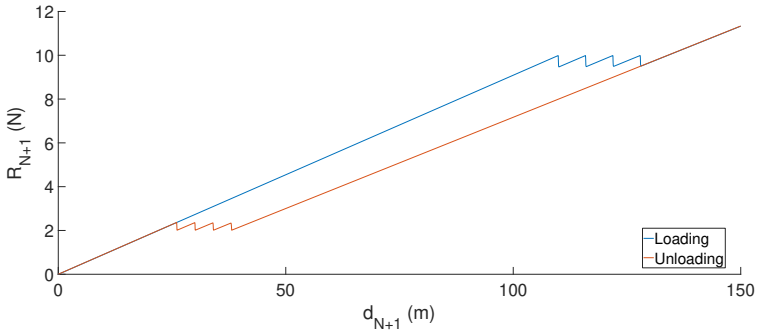

(a) Reaction force evolution ($N = 5, k_N = \frac{k_1}{20}$)

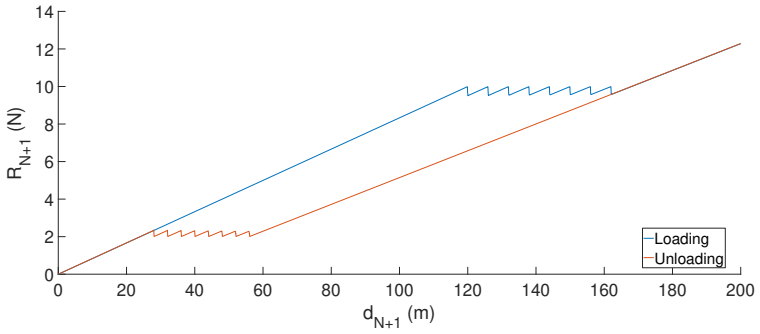

(b) Reaction force evolution ($N = 9, k_N = \frac{k_1}{20}$)

Figure 42: Comparison of the reaction force for different number of piecewise springs ($N = 5$ and $N = 9$)

As it can be seen in Figure 42a and Figure 42b, in both cases the number of peaks equals the number of piecewise springs in each case, as each peak represents the snap-back phenomena for each element. In Figure 43a and Figure 43b, the displacement of each mass is tracked along time. As it can be seen, there is a cascade effect, the first mass snaps first, followed by the others.

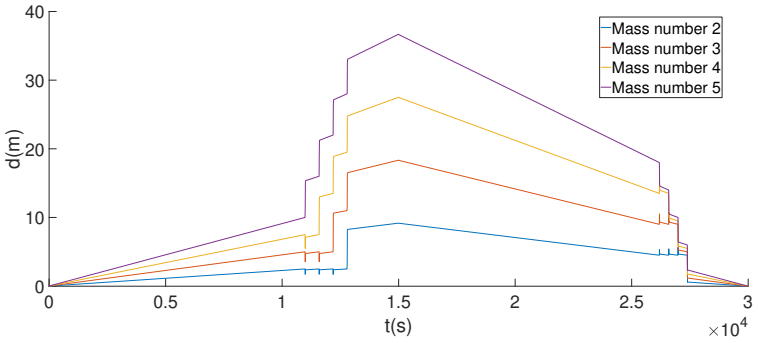

(a) Evolution of the position of each mass along time ($N = 5$, $k_N = \frac{k_1}{20}$)

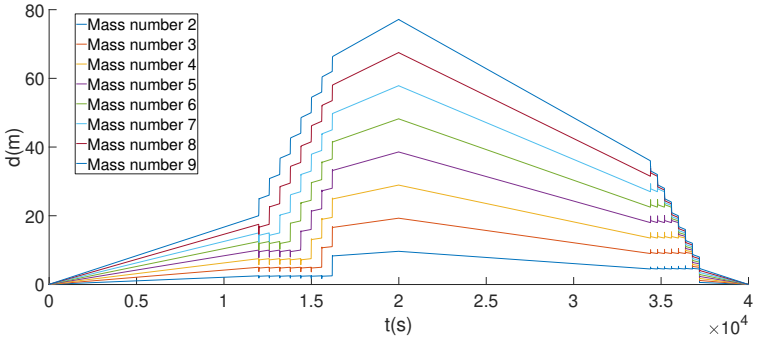

(b) Evolution of the position of each mass along time ($N = 9$, $k_N = \frac{k_1}{20}$)

Figure 43: Comparison of the masses displacement for different number of piecewise springs ($N = 5$ and $N = 9$)

Furthermore, despite looking quite similar, Figure 42a and Figure 42b do have some differences when it comes to its peaks height. If the peaks zone is zoomed in, the following is obtained.

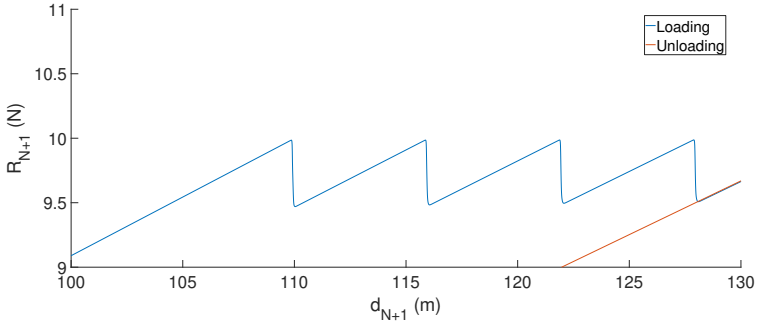

(a) Zoom in the peaks from Figure 42a

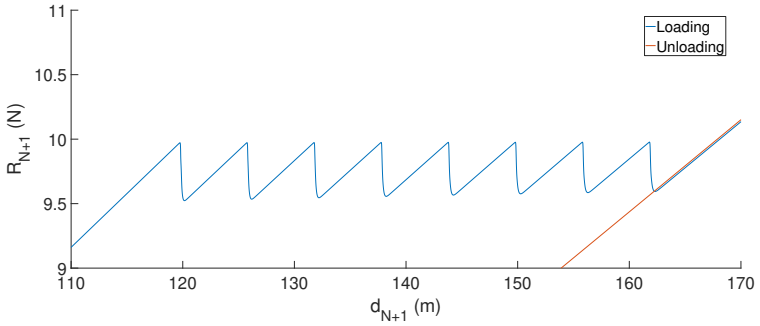

(b) Zoom in the peaks from Figure 42b

Figure 44: Comparison of the peaks height for different number of piecewise springs ($N = 5$ and $N = 9$)

In the $N = 5$ case, the difference between the highest and lowest point of the peak is 0.511 N. On the other hand, in the $N = 9$ case, the difference between the highest and lowest point of the peak is 0.438 N. Therefore, it can be concluded that as the number of springs increase, the peaks become less abrupt. In order to prove this, a further analysis is performed using $N = 21$ and $N = 41$.

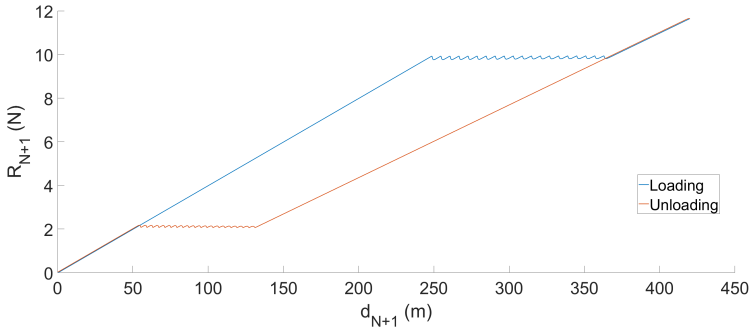

(a) Reaction force evolution ($N = 21$, $k_N = \frac{k_1}{40}$)

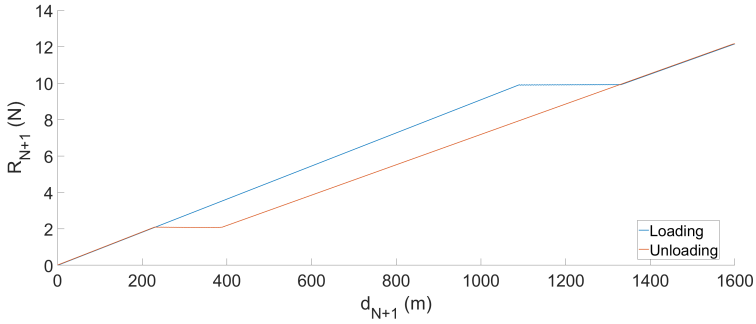

(b) Reaction force evolution ($N = 41$, $k_N = \frac{k_1}{200}$)

Figure 45: Comparison of the reaction force evolution for different number of piecewise springs ($N = 21$ and $N = 41$)

As it can be seen in Figure 45a and Figure 45b, the peaks have been smoothed due to the increase of springs. Once more, a closer look is taken on the peaks in both cases.

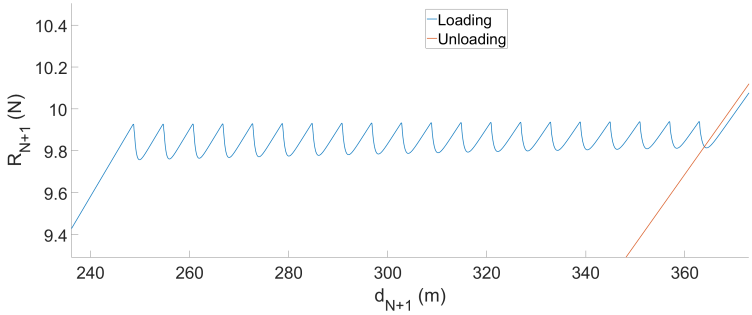

(a) Zoom in the peaks from Figure 45a

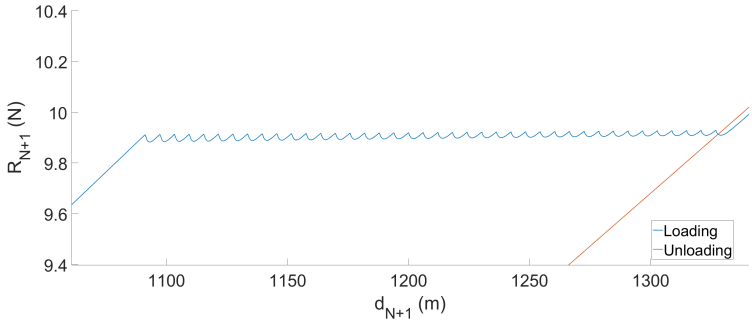

(b) Zoom in the peaks from Figure 45b

Figure 46: Comparison of the peaks height for different number of piecewise springs ($N = 21$ and $N = 41$)

In the $N = 21$ case, the difference between the highest and lowest point of the peak is 0.17 N. On the other hand, in the $N = 41$ case, the difference between the highest and lowest point of the peak is 0.025 N. Additionaly, in the $N = 41$ case, it can be seen that the horizontal lines made of the peaks are placed close to the maximum and minimum values of the element spring (F_{max} and F_{min}).

3.6.1.1 Energy analysis

Again, an energy analysis will be performed. The equations of motion can be written in a matrix form as

$$\boldsymbol{M}\ddot{\boldsymbol{d}} + \boldsymbol{C}\dot{\boldsymbol{d}} + \boldsymbol{F}^{int} = \boldsymbol{R}$$

$$\boldsymbol{M} = \begin{bmatrix} m & 0 & 0 & 0 & 0 \\ 0 & \ddots & 0 & 0 & 0 \\ 0 & 0 & m & 0 & 0 \\ 0 & 0 & 0 & \ddots & 0 \\ 0 & 0 & 0 & 0 & m \end{bmatrix} \qquad \boldsymbol{C} = \begin{bmatrix} c & -c & 0 & 0 & 0 \\ -c & 2c & \ddots & 0 & 0 \\ 0 & \ddots & \ddots & \ddots & 0 \\ 0 & 0 & \ddots & 2c & -c \\ 0 & 0 & 0 & -c & c \end{bmatrix}$$

$$\boldsymbol{F^{int}} = \begin{bmatrix} -f_1(d_2 - d_1) \\ \vdots \\ f_{i-1}(d_i - d_{i-1}) - f_i(d_{i+1} - d_i) \\ \vdots \\ f_N(d_{N+1} - d_N) \end{bmatrix} \qquad \boldsymbol{R} = \begin{bmatrix} R_1 \\ \vdots \\ 0 \\ \vdots \\ R_{N+1} \end{bmatrix}$$

As it has been done before, by multiplying on both sides of the equations by the velocity, the following is obtained

$$\dot{\boldsymbol{d}}^T\boldsymbol{M}\ddot{\boldsymbol{d}} + \dot{\boldsymbol{d}}^T\boldsymbol{C}\dot{\boldsymbol{d}} + \dot{\boldsymbol{d}}^T\boldsymbol{F}^{int} = \dot{\boldsymbol{d}}^T\boldsymbol{R}$$

By replacing the new terms using energy values (U kinetic energy, E_d dissipated energy, E_{int} internal energy, E_R reaction energy), the equation above can be rewritten as

$$\frac{dU}{dt} + \frac{dE_d}{dt} + \frac{dE_{int}}{dt} = \frac{dE_{ext}}{dt}$$

Therefore

$$\frac{dU}{dt} = \dot{\boldsymbol{d}}^T\boldsymbol{M}\ddot{\boldsymbol{d}}$$
$$\frac{dE_d}{dt} = \dot{\boldsymbol{d}}^T\boldsymbol{C}\dot{\boldsymbol{d}}$$
$$\frac{dE_{int}}{dt} = \dot{\boldsymbol{d}}^T\boldsymbol{F}^{int}$$
$$\frac{dE_{ext}}{dt} = \dot{\boldsymbol{d}}^T\boldsymbol{R} = \dot{d}_{N+1}R_{N+1}$$

Taking into account that $\dot{d}_1 = \ddot{d}_1 = \ddot{d}_{N+1} = 0$, the values for each energy during the loading-unloading process can be obtained as follows

- $U = \int_{t_1}^{t_2} \frac{dU}{dt}\, dt$
- $E_d = \int_{t_1}^{t_2} \frac{dE_d}{dt}\, dt$

- $E_{int} = \int_{t_1}^{t_2} \frac{dE_{int}}{dt}\, dt$
- $E_{ext} = \int_{t_1}^{t_2} \frac{dE_R}{dt}\, dt$

As it has been done before, the trapezoidal rule is applied in order to compute the necessary integrals.

Firstly the 5 spring system will be studied, followed by the 9 spring system. In both cases the loading and unloading process will be split.

3.6.1.1.1 5 Spring Sytem

The following values are obtained from the loading process.

- $U = \int_{t_{lim}}^{t_{end}} \frac{dU}{dt}\, dt \longrightarrow \boxed{U = 0 \text{ J}}$
- $E_d = \int_{t_{lim}}^{t_{end}} \frac{dE_d}{dt}\, dt \longrightarrow \boxed{E_d = 91.68 \text{ J}}$
- $E_{int} = \int_{t_{lim}}^{t_{end}} \frac{dE_{int}}{dt}\, dt \longrightarrow \boxed{E_{int} = 864.67 \text{ J}}$
- $E_{ext} = \int_{t_{lim}}^{t_{end}} \frac{dE_{ext}}{dt}\, dt \longrightarrow \boxed{E_{ext} = 956.34 \text{ J}}$

And these values are retrieved from the unloading process.

- $U = \int_{t_{lim}}^{t_{end}} \frac{dU}{dt}\, dt \longrightarrow \boxed{U = 0 \text{ J}}$
- $E_d = \int_{t_{lim}}^{t_{end}} \frac{dE_d}{dt}\, dt \longrightarrow \boxed{E_d = 63 \text{ J}}$
- $E_{int} = \int_{t_{lim}}^{t_{end}} \frac{dE_{int}}{dt}\, dt \longrightarrow \boxed{E_{int} = -864.67 \text{ J}}$
- $E_{ext} = \int_{t_{lim}}^{t_{end}} \frac{dE_{ext}}{dt}\, dt \longrightarrow \boxed{E_{ext} = -801.67 \text{ J}}$

In both cases the following equation is satisfied.

$$U + E_{int} + E_d = E_{ext}$$

Finally, the enclosed area from Figure 42a is calculated using the *trapz* function from *MATLAB*, and the following value is obtained.

$$\text{Enclosed area} = 154.68 \text{ J}$$

Which, indeed, matches the sum of the loading/unloading values of E_d.

$$E_d^{loading} + E_d^{unloading} = 91.68 + 63 = 154.68 \text{ J}$$

3.6.1.1.2 9 spring system

The following values are obtained from the loading process.

- $U = \int_{t_{lim}}^{t_{end}} \frac{dU}{dt}\, dt \longrightarrow \boxed{U = 0 \text{ J}}$
- $E_d = \int_{t_{lim}}^{t_{end}} \frac{dE_d}{dt}\, dt \longrightarrow \boxed{E_d = 182.77 \text{ J}}$
- $E_{int} = \int_{t_{lim}}^{t_{end}} \frac{dE_{int}}{dt}\, dt \longrightarrow \boxed{E_{int} = 1244.57 \text{ J}}$
- $E_{ext} = \int_{t_{lim}}^{t_{end}} \frac{dE_{ext}}{dt}\, dt \longrightarrow \boxed{E_{ext} = 1427.35 \text{ J}}$

And these values are retrieved from the unloading process.

- $U = \int_{t_{lim}}^{t_{end}} \frac{dU}{dt}\, dt \longrightarrow \boxed{U = 0 \text{ J}}$
- $E_d = \int_{t_{lim}}^{t_{end}} \frac{dE_d}{dt}\, dt \longrightarrow \boxed{E_d = 124.68 \text{ J}}$
- $E_{int} = \int_{t_{lim}}^{t_{end}} \frac{dE_{int}}{dt}\, dt \longrightarrow \boxed{E_{int} = -1244.57 \text{ J}}$
- $E_{ext} = \int_{t_{lim}}^{t_{end}} \frac{dE_{ext}}{dt}\, dt \longrightarrow \boxed{E_{ext} = -1119.88 \text{ J}}$

In both cases the following equation is satisfied.

$$U + E_{int} + E_d = E_{ext}$$

Finally, the enclosed area from Figure 42b is calculated using the *trapz* function from *MATLAB*, and the following value is obtained.

$$\text{Enclosed area} = 307.46 \text{ J}$$

Which, indeed, nearly matches the sum of the loading/unloading values of E_d (the difference between the two of them is 0.01 J, which can be considered negligible).

$$E_d^{loading} + E_d^{unloading} = 182.77 + 124.68 = 307.45 \text{ J}$$

3.6.1.2 No damping analysis

Theoretically, if the damping is removed from the system, the whole chain should have a chaotic behaviour as soon as the first spring snaps. To prove this, an analysis is performed using $c = 0$ with 9 springs ($N = 9$).

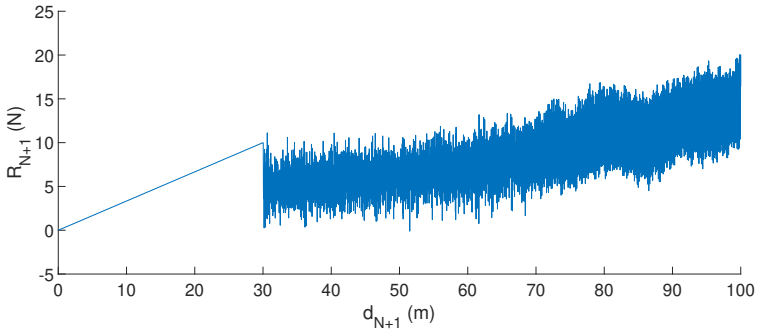

(a) Evolution of the reaction force

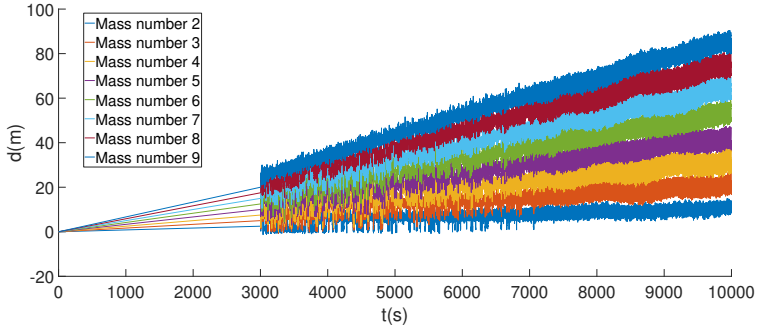

(b) Element mass displacement along time

Figure 47: Overall behaviour of a non-damped system.

Accordingly to what was thought to happen, the system starts oscillating chaotically once the first element snaps.

3.6.2 Bi-stable behaviour

Using similar problem conditions as in the meta-stable case.

$$m = 1\,\text{kg} \quad c = 1\,\text{N s m}^{-1} \quad v_{N+1} = 0.01\,\text{m s}^{-1} \quad k_0 = 4\,\text{N m}^{-1} \quad k_1 = \frac{k_0}{2} \quad k_N = \frac{k_1}{2} \quad F_{max} = 10\,\text{N} \quad F_{max} = -2\,\text{N}$$

The internal force (F_{int}) versus elongation (ϵ) would be then

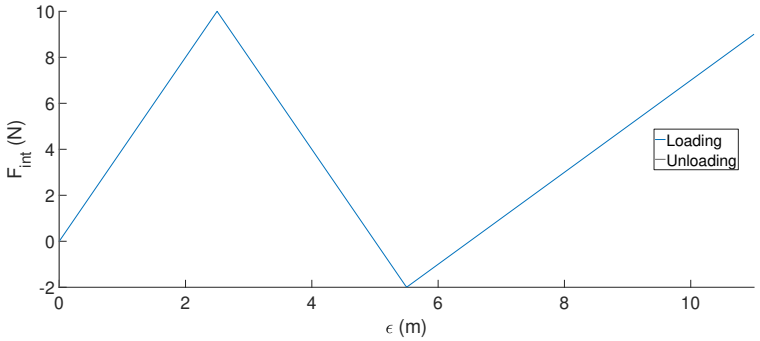

Figure 48: Internal force evolution in the bi-stable case.

The following results are obtained for $N = 5$.

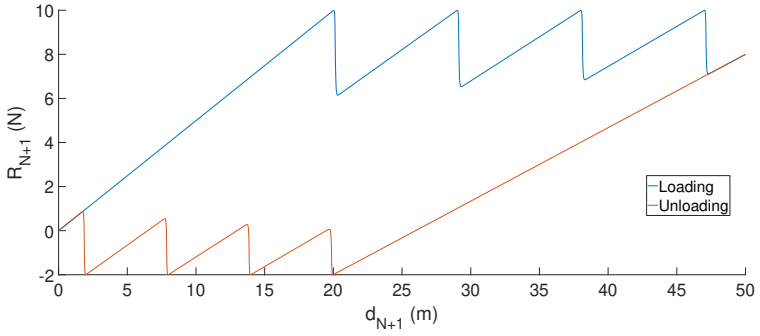

Figure 49: Reaction force evolution ($N = 5$,$k_N = \frac{k_1}{2}$). Bi-stable behaviour

As it can be seen in Figure 49, the behaviour of a chain made up of bi-stable elements is similar to the one that a system made of meta-stable elements has. However, in this case the lower limit is placed on a negative value.

It is worth noting, though that the reaction-displacement graph heavily depends on the value of k_N. These value changes the slope of the unloading path, therefore if it is low enough (for example $k_N = {}^{k_1}/_{20}$), it may happen that when the last mass returns to its original position ($d_{N+1} = 0$ m), not all elements have snapped back, as it is shown below.

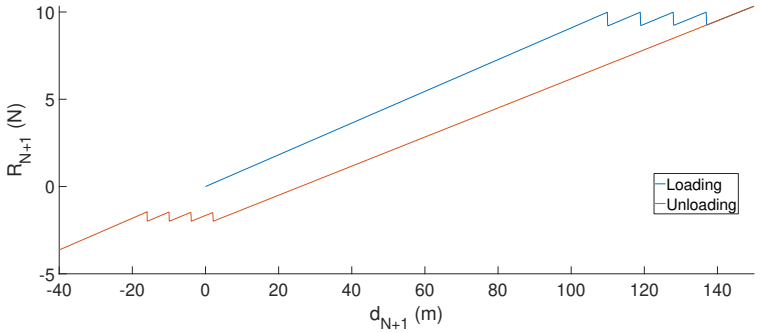

Figure 50: Reaction force evolution ($N = 5$, $k_N = \frac{k_1}{20}$). Bi-stable behaviour

In this case the last mass has to go backwards beyond its initial position so that all springs snap back to their original position. Furthermore, as it has been stated in the meta-stable case, as the number of elements increases, the peaks are smoothed, and the horizontal line is placed at the maximum and minimum value of the internal force. In this case, as the F_{min} is negative, the horizontal value will be placed at -2 N as it is shown below

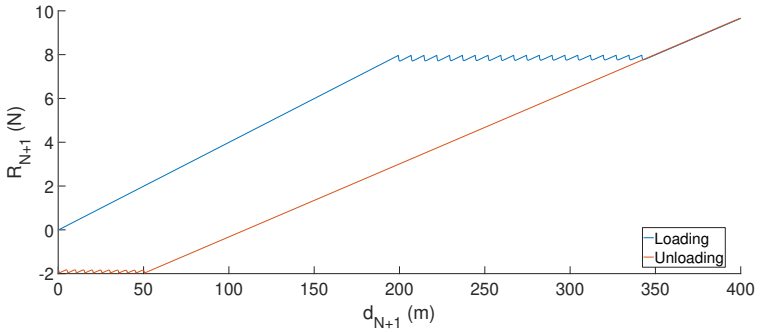

Figure 51: Reaction force evolution ($N = 20$, $k_N = \frac{k_1}{40}$). Bi-stable behaviour

4 Concluding remarks

4.1 Snap-back and snap-through

Firstly, both the snap-through and snap-back phenomena have been properly obtained performing a force-controlled and a displacement-controlled analysis respectively. Comparing what has been obtained (snap-back displayed on Figure 34b; snap-through shown in Figure 25) with the work from other papers

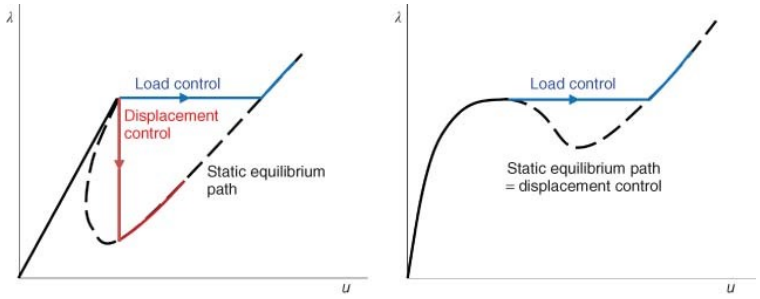

Figure 52: Snap-through and snap-back phenomena depiction. Extracted from [15]

On the one hand, the snap-through phenomena is identical to the right figure from Figure 52. On the other hand, the snap-back phenomena is identical to the left figure from Figure 52 for lower values of k_N. For higher values of k_N the snap-back does not take place (as can be seen on Figure 34b), and the external force follows the internal one.

4.2 Energy damped

Thirdly, it has been checked that a meta-stable element is capable of dissipating energy during its load and unload procedure (Table 6). It has been shown that the energy damped during the loading-unloading process coincides with the area enclosed in Figure 24 [14]. This characteristic of meta-stable element could be really useful in situations where a certain amount of energy has to be dissipated.

4.3 Shape memory effect

Secondly, during the controlled force analysis, it has been seen that, in the bi-stable case, the system does not recover its initial position (Figure 30a) as it does in the meta-stable case. Therefore, it can be concluded that the bi-stable element properly represents the shape memory effect, which is present in *SMART* materials such as Nitinol.

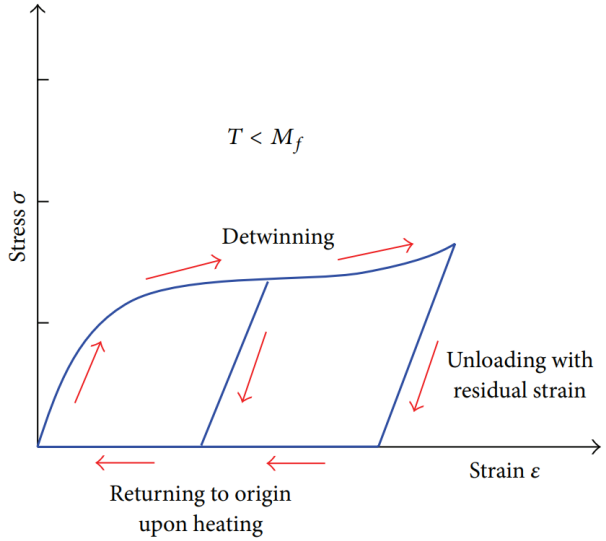

Figure 53: Shape memory effect on a NiTi alloy. Extracted from [8]

Figure 53 is quite similar to what has been obtained in this project (Figure 31). However, in this project no thermal effects have been studied, therefore an implementation of a thermal device on the mass-spring-damper system could lead to the behaviour depicted in Figure 53.

4.4 Chain of multiple elements

Finally, the behaviour of a system made of multiple meta-stable elements has been thoroughly analyzed, and its results show that this assembly represents quite accurately the superelasticity behaviour of *SMART* materials such as Nitinol (50% Nickel, 50% Titanium). Figure 54 contains the typical stress-strain curve of Nitinol. Notice that its shape resembles the one obtained with the 41 meta-stable springs (Figure 45b).

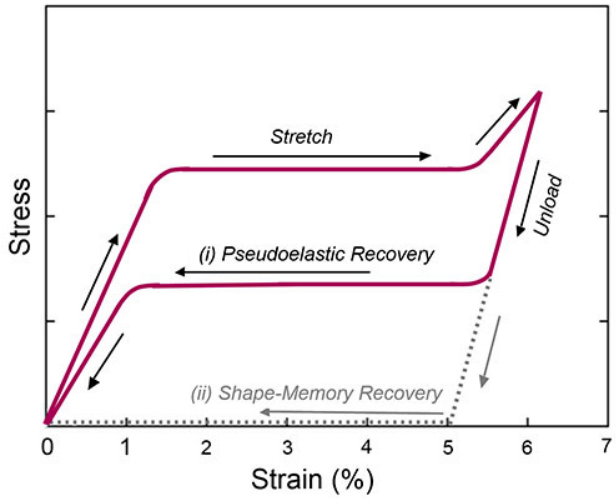

Figure 54: Stress strain curve of a NiTi alloy, showing both its superalisticity and its shape memory. Extracted from [20]

Therefore it can be concluded that an assembly of multiple meta-stable elements depicts quite accurately the stress-strain behaviour of Nitinol as the number of elements in the assembly increases.

References

[1] Pedro M. Reis. A Perspective on the Revival of Structural (In) Stability With Novel Opportunities for Function: From Buckliphobia to Buckliphilia. *Journal of Applied Mechanics, Transactions ASME*, 82(11):1–4, 2015.

[2] David Restrepo, Nilesh D. Mankame, and Pablo D. Zavattieri. Phase transforming cellular materials. *Extreme Mechanics Letters*, 4:52–60, 2015.

[3] Z Wu, R L Harne, and K W Wang. Exploring a modular adaptive metastructure concept inspired by muscle's cross-bridge. *Journal of Intelligent Material Systems and Structures*, 2015.

[4] Chenhui Ren, Deqing Yang, and Haoxing Qin. Mechanical performance of multidirectional Buckling-based Negative Stiffness metamaterials: An analytical and numerical study. *Journal of Materials*, 11(7), 2018.

[5] Benjamin Jenett, Sam Calisch, Daniel Cellucci, Nick Cramer, Neil Gershenfeld, Sean Swei, and Kenneth C. Cheung. Digital Morphing Wing: Active Wing Shaping Concept Using Composite Lattice-Based Cellular Structures. *Soft Robotics*, 4(1):33–48, 2017.

[6] David L Chandler. MIT and NASA engineers demonstrate a new kind of airplane wing, 2019. http://news.mit.edu/2019/engineers-demonstrate-lighter-flexible-airplane-wing-0401, Last accesed on 16-06-2020.

[7] Itamar Benichou and Sefi Givli. Structures undergoing discrete phase transformation. *Journal of the Mechanics and Physics of Solids*, 61(1):94–113, 1 2013.

[8] Hui Qian, Hongnan Li, Gangbing Song, and Wei Guo. Recentering shape memory alloy passive damper for structural vibration control. *Mathematical Problems in Engineering*, 2013, 2013.

[9] Nan Hu and Rigoberto Burgueño. Buckling-induced smart applications: Recent advances and trends. *Smart Materials and Structures*, 24(6), 2015.

[10] Bruno Ando, Salvatore Baglio, Adi R. Bulsara, Vincenzo Marletta, Vittorio Ferrari, and Marco Ferrari. A low-cost snap-through-buckling inkjet-printed device for vibrational energy harvesting. *IEEE Sensors Journal*, 15(6):3209–3220, 2015.

[11] Glenn A. Hrinda. Snap-through instability patterns in truss structures. *Collection of Technical Papers - AIAA/ASME/ASCE/AHS/ASC Structures, Structural Dynamics and Materials Conference*, pages 1–12, 2010.

[12] Itamar Benichou, Yaojun Zhang, Olga K. Dudko, and Sefi Givli. The rate dependent response of a bistable chain at finite temperature. *Journal of the Mechanics and Physics of Solids*, 95:44–63, 10 2016.

[13] Ahmad Rafsanjani, Abdolhamid Akbarzadeh, and Damiano Pasini. Snapping Mechanical Metamaterials under Tension. *Advanced Materials*, 27(39):5931–5935, 10 2015.

[14] Mansour Alturki and Rigoberto Burguen. Multistable Cosine-Curved Dome System for Elastic Energy Dissipation. *Journal of Applied Mechanics*, 2019.

[15] Manfred Bischoff, E. Ramm, and J. Irslinger. Models and Finite Elements for Thin-Walled Structures. In *Encyclopedia of Computational Mechanics Second Edition*, pages 1–86. John Wiley & Sons, Ltd, Chichester, UK, 12 2017.

[16] Donald Greenspan. Runge-Kutta Methods. *Numerical Solution of Ordinary Differential Equations*, pages 11–36, 2008.

[17] S. Rajasekaran. *Structural dynamics of earthquake engineering: theory and application using Mathematica and Matlab*. Woodhead, 2009.

[18] H. Hashamdar, Z. Ibrahim, and M. Jameel. Finite element analysis of nonlinear structures with Newmark method. *International Journal of Physical Sciences*, 6(6):1395–1403, 2011.

[19] Wook Bae Kim and Sol Yi Han. Microinjection molding of out-of-plane bistable mechanisms. *Micromachines*, 11(2), 2020.

[20] MedShape INC. NiTiNOL Implants | Nickel Titanium, 2019. https://www.medshape.com/technology/shape-memory-alloy/, Last accesed on 16-06-2020.

[21] Yair Altman. ExportFig MATLAB package, 2020. https://www.github.com/altmany/export_fig, Last accesed on 24-06-2020.

List of Figures

All figures that are not referenced have been created using *MATLAB* software.[21]

List of Tables